Covalent inhibitors of EGFR family protein kinases induce degradation of human Tribbles 2 (TRIB2) pseudokinase in cancer cells

Daniel M. Foulkes[1], Dominic P. Byrne[1], Wayland Yeung[2], Safal Shrestha[2], Fiona P. Bailey[1], Samantha Ferries[1,3], Claire E. Eyers[1,3], Karen Keeshan[4], Carrow Wells[5], David H. Drewry[5], William J. Zuercher[5,6], Natarajan Kannan[2] and Patrick A. Eyers[1]*

[1] Department of Biochemistry, Institute of Integrative Biology, University of Liverpool, L69 7ZB, UK

[2] Institute of Bioinformatics and Department of Biochemistry & Molecular Biology, University of Georgia, Athens, GA 30602, USA

[3] Centre for Proteome Research, Institute of Integrative Biology, University of Liverpool, L69 7ZB, UK

[4] Paul O'Gorman Leukaemia Research Centre, Institute of Cancer Sciences, University of Glasgow, Scotland, UK

[5] Structural Genomics Consortium, UNC Eshelman School of Pharmacy, University of North Carolina at Chapel Hill, Chapel Hill, NC, 27599, USA

[6] Lineberger Comprehensive Cancer Center, University of North Carolina at Chapel Hill, Chapel Hill, NC 27599, USA

* Correspondence to Patrick.eyers@liverpool.ac.uk

ABSTRACT:

A major challenge associated with biochemical and cellular analysis of pseudokinases is a lack of target-validated small molecule compounds with which to probe function. Tribbles 2 (TRIB2) is a cancer-associated pseudokinase with a diverse interactome, including the canonical AKT signaling module. There is substantial evidence that human TRIB2 promotes survival and drug-resistance in solid tumors and blood cancers and therefore is of interest as a therapeutic target. The unusual TRIB2 pseudokinase domain contains a unique cysteine-rich C-helix and interacts with a conserved peptide motif in its own C-terminal tail, which also supports its interaction with E3 ubiquitin ligases. Here, we found that TRIB2 is a target of previously described small molecule protein kinase inhibitors, which were originally designed to inhibit the canonical kinase domains of epidermal growth factor receptor (EGFR) tyrosine kinase family members. Using a thermal-shift assay (TSA), we discovered TRIB2-binding compounds within the Published Kinase Inhibitor Set (PKIS), and used a drug repurposing approach to classify compounds that either stabilized or destabilized TRIB2 in vitro. TRIB2 destabilizing agents, including the covalent drug afatinib, led to rapid TRIB2 degradation in human

AML cancer cells, eliciting tractable effects on signaling and survival. Our data reveal new drug leads for the development of TRIB2-degrading compounds, which will also be invaluable for unravelling the cellular mechanisms of TRIB2-based signaling. Our study highlights that small molecule-induced protein downregulation through drug "off-targets" might be relevant for other inhibitors that serendipitously target pseudokinases.

INTRODUCTION:

The human protein kinome encodes ~60 protein pseudokinases, which lack at least one conventional catalytic residue, but often control rate-limiting signaling outputs within cellular networks [1]. Like canonical kinases, pseudokinases drive conformation-dependent signaling associated with both physiology and disease [2, 3]. The human 'pseudokinome' includes cancer-associated signaling proteins such as human epidermal growth factor receptor 3 (HER3), Janus kinase 2 (JAK2; JH2 domain) and Tribbles 2 (TRIB2), which have received much less attention than their conventional, catalytically-active counterparts even though pseudokinase domains represent rational targets for drug discovery [4]. Discovering or repurposing biologically and/or clinically-active compounds that target atypical-conformations of canonical kinases or pseudokinases, is an area of active research [2, 3, 5-9]. Moreover, the burgeoning pseudokinase field is strongly placed to benefit from the decades of research undertaken on canonical protein kinases, which has seen the approval of over 40 kinase inhibitors for human cancer and inflammatory diseases [10, 11]. This includes understanding how ATP-competitive, allosteric, or covalent inhibitors might influence pseudokinase-based signaling mechanisms that are relevant to health and disease [3, 12].

The three human TRIB pseudokinases (TRIB1, TRIB2, and TRIB3) and the related pseudokinase STK40 (serine/threonine kinase 40, also known as SgK495) are homologues of the *Drosophila melanogaster* pseudokinase termed Tribbles, which controls ovarian border cell and neuronal stem cell physiology in flies [13, 14] These proteins contain a catalytically-impaired pseudokinase domain. Adaptions in the pseudokinase fold, including a highly unusual αC-helix, are thought to support a competitive regulatory interaction *in cis* with a unique C-terminal tail DQLVP motif [15-17]. Through a still obscure mechanism, TRIB and STK40 function as adaptor proteins that recruit ubiquitin E3 ligases, such as constitutive photomorphogenesis protein 1 homolog (COP1), through interaction with the conserved C-tail peptide [15, 17], which is also required for signaling and cellular transformation [18]. Mechanistically, Tribbles proteins' signaling outputs are controlled through the ubiquitylation and subsequent proteasomal destruction of Tribbles 'pseudosubstrates"; in vertebrates, these include the transcription factor C/EBPα, the cell cycle-associated phosphatase CDC25C, and the enzyme acetyl CoA carboxylase [19-21].

A longstanding goal in cancer research is drug-induced degradation of oncogenic proteins. Progress towards this objective has been transformed by the synthesis of proteolysis-targeting chimeras

(PROTACs), which induce proteasome-dependent degradation of their targets. Multifunctional small molecule PROTACS often possess protein-binding regions derived from kinase inhibitors [22, 23], and multiple classes of non-PROTAC kinase inhibitor also induce kinase target degradation, although typically at higher (micromolar) concentrations than those required for enzymatic inhibition [7]. Recent reports also disclose classes of covalent compounds that bind and disable cysteine (Cys)-containing small G-proteins such as mutant human RAS, permitting covalent inactivation of this previously 'undruggable' oncoprotein [24, 25]. Cys residues are widespread and highly conserved in kinases [26] and the conservation of Cys residues both inside and outside the catalytic domain provides kinome-wide opportunities for exploitation using chemical biology [27]. In this context, covalent targeting methodologies involving compound-accessible Cys residues in kinases [8, 28-31] and pseudokinases [3], have attracted significant attention for small molecule design, due to the potential for gains in target specificity and durability of responses, combined with tractability in experimental systems.

Tribbles pseudokinases are implicated in many physiological signaling pathways, often in the context of protein stability, but also through regulation of key modules, such as the canonical AKT pathway [32]. TRIB2 is also implicated in the aetiology of human cancers, including leukemias, melanoma, and lung and liver cancers [33]. In particular, TRIB2 is a potential drug target in subsets of acute myeloid and lymphoid leukemia (AML and ALL), which are in urgent need of targeted therapeutics to help treat untargeted or drug-resistant patient populations [34]. TRIB2 protein abundance has also been linked to drug-resistance mechanisms, where an ability to modulate the pro-survival AKT signaling module underlies a central regulatory role in cell proliferation, differentiation, metabolism, and apoptosis [32, 35-39].

Here, we found that the low-affinity ATP-binding site in TRIB2 [40] was druggable with small molecules previously described as ATP-competitive pan-EGFR family kinase inhibitors. Biochemical analysis confirmed the existence of distinct compound-induced TRIB2 conformations and a compound screen identified known EGFR family inhibitors that stabilize or destabilize TRIB2 *in vitro*. TRIB2-binding compounds included the clinically used breast cancer therapeutic lapatinib (marketed as Tykerb) [41] and the FDA-approved irreversible electrophilic covalent inhibitors afatinib (Giotrif) [42, 43] and neratinib (Nerlynx) [44, 45]. In the case of the latter two destabilizing agents, binding led to uncoupling of the pseudokinase domain from its own C-terminal tail. Consistently, afatinib exposure led to rapid TRIB2 degradation in cells, driven by an interaction with the Cys-rich pseudokinase domain, which interfered with AKT signaling and decreased cell survival in a TRIB2-expressing leukemia model. The availability of target-validated compounds that act as rapid TRIB2 pseudokinase down-regulators *via* a direct effect on the pseudokinase represents a new way to evaluate TRIB2 physiology and cell signaling. It might also have a broader impact on the

rapidly developing pseudoenzyme field [46], where the concept of pseudokinase destabilization or elimination by targeted kinase ‘inhibitors’ [7] has a number of potentially useful applications.

RESULTS:

Analysis of human TRIB2 using a thermal stability assay

Human TRIB2 differs from TRIB1, TRIB3 and STK40 in the pseudokinase domain due to a Cys-rich region at the end of the β3 Lys-containing motif leading into the truncated αC-helix in the N-lobe (Fig. 1A, top). We developed a differential scanning fluorimetry (DSF) assay [47-49] to examine thermal stability of full-length (1-343) His-tagged TRIB2 proteins, and compared it either to full-length cAMP-dependent protein kinase (PKAc) catalytic subunit, which is a model for canonical kinases, or full-length C104Y TRIB2, in which Cys^{104} was replaced with the Tyr residue conserved in human TRIB1 and TRIB3 (Fig. 1A). Proteins were purified to homogeneity (Fig. 1A, bottom) and thermal stability based on unfolding profiles were determined for each protein (reported as a T_m value, Fig. 1B). As previously demonstrated [40], TRIB2 (T_m = ~39 °C) was much less thermostable than the canonical protein kinase (PKA, T_m = 46.3 °C). Remarkably, the C104Y single substitution induced stabilization of TRIB2, with the T_m value increasing to ~49 °C, comparable to that of human TRIB1 [15], suggesting an important structural role for this unique Cys residue in TRIB2 (un)folding dynamics. To confirm that recombinant TRIB2 binds to a known physiological target, we demonstrated that GST-tagged TRIB2 interacted preferentially with catalytically inactive (non Thr^{308}-phosphorylated) AKT1 *in vitro* (Fig. 1C). Consistent with a functional regulatory interaction between TRIB2 and AKT in cells [50], transient overexpression of TET-inducible FLAG-tagged TRIB2 in HeLa cells led to a large increase in endogenous AKT phosphorylation at the hydrophobic motif (Ser^{473}, Fig. 1D), an established marker for AKT catalytic activity and generation of a downstream cellular anti-apoptotic signal [51].

A DSF screen for TRIB2-binding compounds using a kinase inhibitor library

The ability of full-length recombinant human TRIB2 to bind to adenosine triphosphate (ATP) in the presence of EDTA [40, 48] confirms that a vestigial nucleotide-binding site is present within the pseudokinase domain. Moreover, our previous work established that an analogue-sensitive (F190G) TRIB2 variant could be stabilized by bulky pyrimidine analogues *in vitro* [40]. To discover drug-like compounds for WT (full-length) TRIB2, we screened the Published Kinase Inhibitor Set (PKIS), a collection of high-quality class-annotated kinase inhibitors [52]. We enforced cut off values of ~ΔT_m = < -2 °C and > +3.5 °C (therefore eliminating ~97% of the library) to define 'hit' compounds that possessed the ability to destabilize or stabilize TRIB2 in a thermal stability assay (TSA) at a 1:4 TRIB2:compound molar ratio (Fig. 1E and table S1). The top 'stabilizing' compound identified was GW693881A, a dual EGFR and HER2 thienopyrimdine inhibitor with a ΔT_m of +4.7 °C. The top 'destabilizing' compound was GW804482X, a thiophene polo-like kinase (PLK) inhibitor that induced a ΔT_m of - 3.4 °C (Fig. 1E, red symbols). Most of the top stabilizing and destabilizing

compounds belonged to well-known ATP-competitive pyrimidine or quinazoline EGFR family chemotypes (fig. S1) [53-55], suggesting broad structural cross-reactivity between TRIB2 and a compound-binding EGFR and HER2 conformation. To build upon these findings, we screened a larger panel of known dual EGFR and HER2 inhibitors (fig. S2), and established that the clinical type I EGFR family inhibitors TAK-285 and lapatinib also stabilized TRIB2 *in vitro* (Fig. 1F). The ATP-competitive covalent EGFR family inhibitors afatinib, neratinib and osimertinib (but not the unrelated covalent Bruton's Tyrosine Kinase (BTK) inhibitor ibrutinib or the Type I EGFR-specific inhibitors erlotinib or gefitinib) destabilized TRIB2, similar to the PLK inhibitor GW804482X (Fig. 1F) and the dual EGFR family inhibitor GW569530A (fig. S1). As expected [15], purified TRIB1 (fig. S3A) was more thermostable than TRIB2 in the absence of kinase inhibitors (fig. S3B). However, it was not destabilised by afatinib, neratinib or osimertinib, although like TRIB2, destabilisation was evident in the presence of GW804482X (fig. S3C), in agreement with independent findings [56]. Compound effects were caused through pseudokinase targeting in the TSA, because no shift was elicited when the canonical kinase PKAc was compared in a side-by-side counter-screen, with dasatinib as a positive control (fig. S3D). The preclinical PLK inhibitors BI2536 and BI6727 (volasertib) had no discernible effects on TRIB2 stability in this assay, in contrast to the chemically distinct thiophene PLK inhibitor GW804482X (Fig. 1F).

Afatinib, neratinib and osimertinib are covalent (type IV) inhibitors of EGFR family tyrosine kinases, interacting irreversibly with a conserved Cys residue in the canonical ATP-binding site [57]. The stabilization of TRIB2 by lapatinib, and the destabilization of TRIB2 by all three covalent inhibitors, occurred in a dose-dependent manner (Fig. 1G and fig. S4). A C104Y TRIB2 mutant was no longer destabilized by either afatinib or neratinib, but remained 'sensitive' to lapatinib TAK-285 and GW804482X based on thermal-protection (Fig. 1H and fig. S5A). Importantly, none of these latter compounds contain the electrophilic 'warhead' required for covalent interactions (fig. S2). Elution profiles from Superdex 200 were identical for WT and C104Y TRIB2 (fig. S5B), confirming that both proteins were monomeric species in solution, with estimated M*r* of 45.3 kDa. C104Y TRIB2 was also insensitive to thermal shift in the presence of ATP and EDTA (Fig. 1H and fig. S5C). These data suggest that the amino acid identity at TRIB2 position 104 is likely important both for ATP binding and interaction with covalent kinase inhibitors that induce TRIB2 destabilization *in vitro*.

Mechanistic analysis of TRIB2 structural stability and TRIB2 compound binding

Structural analysis of TRIB1 by X-ray crystallography and small angle X-ray scattering led to the proposal of an *in cis* self-assembly model, whereby the unique C-terminal tail region, which contains the conserved 'DQLVP' motif, binds directly to the pseudokinase domain adjacent to the short αC-helix of TRIB1 [15, 16, 56]. To investigate whether this mechanism is also relevant in TRIB2, we generated a series of truncated proteins. These lacked either the N-terminal extension, which was

predicted to be disordered by both I-TASSER [58] and VSL2 [59], the C-terminal tail, or both N and C-terminal regions. We also generated a triple point mutant in which the 'DQLVP' tail motif, which is required for TRIB1 and TRIB2 cellular transformation *in vivo* [18], was mutated to a non-functional 'AQLAA' sequence (Fig. 2A). Full-length (1-343) TRIB2, and TRIB2 lacking the N-terminal domain (TRIB2 54-343), both exhibited similar T_m values of 39-40 °C (Fig. 2B). In contrast, deletion of the C-tail (TRIB2 1-318) changed TRIB2 stability, with T_m values falling to ~37°C, diagnostic of a destabilized TRIB2 conformation (Fig. 2B). Mutation of DQLVP to AQLAA further destabilized TRIB2, leading to a T_m value of ~36 °C (Fig. 2B). Using this panel of recombinant TRIB2 proteins, we measured the relative effects of kinase inhibitors on TRIB2 stability. Consistent with a lack of effect on compound interactions, deletion of the TRIB2 N-terminal region had no effect on ΔT_m values induced by any compound. However, removal of the C-tail region (54-318 and 1-318 mutants) abolished afatinib and neratinib-induced TRIB2 destabilization, but had a negligible effect on GW804482X binding (Fig. 2C). Consistently, destabilization by afatinib was also completely abolished in the AQLAA triple mutant, whereas neratinib effects were reduced by >50%. Notably, neither the destabilizing effect of GW804482X, nor the stabilizing effects of lapatinib or TAK-285 differed between any of the TRIB2 proteins evaluated. These results suggest a very similar destabilizing mechanism induced by covalent EGFR family compounds *via* displacement of the TRIB2 C-tail, which is a unique feature of Tribbles pseudokinases [13, 15].

To evaluate whether afatinib targeted unique Cys residues in the TRIB2 pseudokinase domain (Fig. 1A), we performed mass spectrometry (MS) analysis to evaluate protein modification. As detailed in fig. S6A, incubation of TRIB2 with a 5-fold molar excess of afatinib led to covalent interaction with Cys 96 in TRIB2. A doubly charged chymotryptic product ion representing the TRIB2-derived DISC^{96}Y:afatinib peptide adduct at *m/z* 543.2 (fig. S6A) and the isotopic ratios of the ^{35}Cl or ^{37}Cl-containing peptide ions unequivocally confirmed Cys^{96} as a site of TRIB2 binding (fig. S6B). Having confirmed an intact mass for recombinant full-length TRIB2 of 43,587.09 Da, very similar to the predicted mass of 43,587.22 Da (fig. S6C), we were also able to ascertain that pre-incubation with afatinib generated covalent adducts containing predominantly either 1 or 2 molecules of afatinib. There was also some evidence for tri and tetra-modified TRIB2 adducts (fig. S6D). We next examined afatinib interaction with TRIB2 by Microscale Thermophoresis (MST), a biophysical technique for quantification of reversible biomolecular interactions [60]. This revealed an interaction between fluorescent NTA-coupled His-TRIB2 and two compounds, which could be fitted to reversible binding with K*d* values of ~16 μM for afatinib and ~20 μM for TAK-285 (fig. S7, A and B). A sub-micromolar interaction between MCL-1 and A1210477 served as a positive control [61]. In agreement with MS data (fig. S6), we therefore propose initial (reversible) binding of ATP-competitive afatinib [62, 63], prior to subsequent formation of a covalent adduct(s) with the TRIB2 pseudokinase domain. We also evaluated the potential interaction of afatinib and neratinib using TRIB2 modelled on the

C/EBP-bound 'SLE-in' conformation from TRIB1 [13, 56] and compared it to the known afatinib target EGFR (in a 'DFG-in' conformation) using AutoDock Vina [64]. Docking of covalent inhibitors revealed a putative binding pocket formed by residues from the vestigial TRIB2 C-helix, including Cys^{96}, and the β3 strand (fig S8A). Afatnib and neratinib dock in a structurally similar pose in which the enamine beta carbon orients towards the sulfhydryl group of Cys^{96}. This docking pose, however, is distinct from the afatinib-bound crystal structure of EGFR, wherein Cys^{797} is located in the D-helix. We performed molecular dynamics simulations (fig. S8B) on the docked complexes to assess the feasibility of the binding poses. Both afatinib and neratinib remained stably bound to TRIB2 for nearly 17 ns, suggesting that the binding poses are favorable and feasible. [65]. The enamine beta carbon remained within 3-5 Å of the Cys^{96} sulfur atom for the majority of the simulation. Given the rapid nature of the thiol-ene reaction coupled with the proximity of reactants, we believe that this time frame offers sufficient time for the formation of a covalent bond [66], which we confirmed by MS analysis.

To validate the biochemical importance of Cys residues for afatinib binding, we next examined interaction with TRIB2 in which two Cys amino acids were mutated to non-thiol containing Ser residues. Individual or combined mutation of Cys^{96} and Cys^{104} to a Ser residue had no effect on the thermal stability (T_m) of the purified TRIB2 proteins (Fig. 2D), in contrast to the highly stabilizing effect of a Tyr at position 104 (Fig. 1B and fig. S5C). However, individual or joint mutation of $Cys^{96}$and Cys^{104} to Ser severely blunted the destabilizing effect of afatinib and neratinib on TRIB2, in contrast to the non-covalent TRIB2 compound GW804482X or the EGFR family stabilizing compounds lapatinib and TAK-285 (Fig. 2E). Together, our findings confirm that these covalent compounds elicit effects on TRIB2 through Cys96 and/or Cys^{104}.

Evaluation of TRIB2 interactors in human cells

To evaluate TRIB2 targeting by compounds in living cells, we generated a polyclonal TRIB2 antibody and an isogenic stable HeLa cell line expressing TET-inducible FLAG-tagged human TRIB2. Polyclonal TRIB2 antibodies were equally efficient at recognising recombinant His-FLAG-TRIB2 and cellular FLAG-TRIB2 as a commercial monoclonal FLAG antibody (fig. S9A). We also constructed a stable HeLa cell line expressing low levels of inducible FLAG-TRIB2 (fig. S9B). We estimated that ~1 ng of TRIB2 was expressed in 40 μg of whole cell lysate in the presence of TET, by comparing known amounts of recombinant His-FLAG-TRIB2 protein (fig. S9B).

To quantify effects of TRIB2 expression on canonical signaling in model cells, we evaluated AKT phosphorylation. AKT became phosphorylated in stable HeLa cells after serum stimulation in the absence of TET (Fig. 3A). TRIB2 expression led to the appearance of a TRIB2 doublet (phosphorylation confirmed in the upper band by lambda phosphatase treatment, fig. S10), and a

marked increase in the extent and duration of AKT phosphorylation at Ser^{473}. Using this HeLa cell model, we next evaluated the effects of small molecule inhibitors on TRIB2 signaling, by comparing a panel of *in vitro* TRIB2 destabilizing compounds discovered by DSF (afatinib, neratinib and osimertinib) with a series of control compounds. Brief (4 hours) exposure of TRIB2-expressing cells to afatinib led to a specific decrease in TRIB2 protein expression. All of the compounds evaluated were specific EGFR or EGFR family signaling pathway inhibitors, and consistently they all blocked ERK phosphorylation at these concentrations (Fig. 3B); any unique effects of drugs amongst this panel are therefore likely to be 'off-target' to EGFR and HER2. We next incubated cells for increasing lengths of time with afatinib. A rapid, time-dependent, elimination of TRIB2 protein was evident when cells were exposed to this drug, in contrast to DMSO controls in which TRIB2 protein remained relatively stable during the experiment (Fig. 3C), as expected [19]. To evaluate intracellular interaction between TRIB2 and kinase inhibitors, we exposed HeLa cells expressing TET-inducible FLAG-TRIB2 to each compound, and quantified TRIB2 thermal stability in the cell extracts using a cellular TSA (fig. S11) [67]. Consistently, FLAG-TRIB2 was destabilized more rapidly than DMSO and erlotinib-treated controls in the presence of afatinib, becoming undetectable in extracts heated to 45 °C (fig. S11). This was distinct from lapatinib, which partially stabilized TRIB2 in cell extracts, consistent with our *in vitro* analysis (Fig. 1F).

Afatinib interacts with TRIB2 through a biochemical Cys-based mechanism, so we generated isogenic TET-inducible C96S or C96/104S TRIB2-mutant stable cell lines (fig. S12) and evaluated the effects of afatinib on exogenous TRIB2 stability. Afatinib (but not lapatinib or TAK-285) induced dose-dependent loss of TRIB2 in WT-TRIB2 cells, which was partially prevented for C96S, and completely abolished in C96/104S TRIB2-expressing cells (quantified in Fig. 4A, right panels), demonstrating unequivocally that afatinib binds to TRIB2 in cells. Furthermore, afatinib (but not TAK-285 or erlotinib) treated WT-TRB2 cells exhibited a marked decrease in AKT Ser^{473} phosphorylation, and this effect was abrogated in C96/104S TRIB2-expressing cells (Fig. 4B). Importantly, afatinib, TAK-285, and erlotinib all blocked ERK phosphorylation in WT and C96/104S-TRIB2 isogenic cell lines, consistent with 'on-target' inhibition of their shared EGFR target (Fig. 4B).

To investigate the mechanism of TRIB2 destabilization by afatinib, we added the drug to HeLa cells expressing WT-TRIB2 in the presence of the proteasome inhibitor MG132, which partially rescued TRIB2 degradation after both rapid and prolonged exposure to afatinib (Fig. 4C). This finding is consistent with previously reported proteasome-dependent TRIB2 turnover [68]. We further evaluated this mechanism using a range of MG132 concentrations and the clinical proteasome inhibitor bortezomib (Fig. 4D) [21]; under both conditions, afatinib-mediated destabilization of TRIB2 was decreased. This effect was in contrast to afatinib-induced TRIB2 destabilization, which was still observed in the presence of non-specific inhibitors of autophagy (AICAR) and lysosomal degradation (chloroquine) (Fig. 4D). Our observations are in line with published findings, which suggest that

TRIB2 fate is dependent upon turnover by the ubiquitin proteasome system (UPS) in human cancer cells [19, 69]. However, the (non-covalent) TRIB1 and TRIB2-destabilizing compound GW804482X did not induce TRIB2 degradation in cells after a 4-hour incubation period, in contrast to proteasome-dependent degradation induced by the same concentration of afatinib (fig. S13).

High expression of TRIB2 drives AML *in vivo* by inhibiting myeloid differentiation and promoting proliferation [18, 35]. However, endogenous TRIB2 expression has been analysed previously only in a few cell types, in large part due to a lack of reliable TRIB2 reagents. Using our TRIB2 antibody, we evaluated endogenous expression of TRIB2 in the clinically-relevant U937 AML cell model (Fig. 5A), and established that acute (4 hours) exposure to afatinib, but not lapatinib or erlotinib, decreased TRIB2 protein abundance in a dose-dependent manner (Fig. 5A). Consistent with their ability to inhibit EGFR signaling, all three compounds completely blocked ERK phosphorylation. We next established dose-dependent effects on both TRIB2 expression and AKT Ser^{473} phosphorylation in afatinib-treated U937 cells (Fig. 5B). Notably, these effects were tightly correlated with apoptotic induction of caspase 3 cleavage, but only at afatinib concentrations that also induced TRIB2 degradation and concomitant loss of AKT Ser^{473} phosphorylation (Fig. 5B). To determine the impact of afatinib treatment on U937 cell viability, we quantified cellular cytotoxicity after 72 hours exposure (Fig. 5C). Afatinib (and neratinib) reduced cell viability with sub-micromolar IC_{50} values, whereas EGFR inhibitors erlotinib and gefitinib and the dual EGFR family inhibitor TAK-285 were comparably 10-20–fold less effective (Fig. 5C). Because these compounds do not induce cellular TRIB2 destabilization, AKT activation or caspase 3 activation, our data suggest that the TRIB2-destabilizing compounds afatinib and neratinib possess an enhanced ability to kill AML-derived cells [50].

DISCUSSION:

A drug-targetable regulatory mechanism for human TRIB2

Cell Signaling can be controlled by non-enzymatic components, exemplified by mechanistically-related families of pseudoenzymes such as pseudokinases [46]. In this study, we sought to target the cancer-associated pseudokinase TRIB2 with a chemical small molecule. To discover TRIB2-binding compounds, we exploited an unbiased TRIB2 thermal shift assay [40, 48], and identified multiple chemical classes of EGFR family member (typically EGFR and HER2, but never monovalent EGFR) kinase inhibitors. Several compounds induced stereotypical (positive) thermal shifts in TRIB2, consistent with binding in the atypical nucleotide-binding site [48]. A second compound group led to marked TRIB2 (but not TRIB1) destabilization, and this could be explained through a Cys-directed covalent effect, in which the TRIB2 pseudokinase domain became uncoupled from its own C-tail by the compound. A similar mechanism has recently been proposed to explain thermally-distinct conformers in TRIB1, which shares ~70% identity with TRIB2 in the pseudokinase domain and C-tail [16]. Deletion of the TRIB1 C-tail also leads to destabilization of the TRIB1 pseudokinase domain [15], similar to the effects observed for TRIB2 described here. These data allow us to propose that TRIB2 pseudokinase-domain docking to the C-terminal tail is a dynamic interaction, which can be targeted with covalent ATP-competitive covalent inhibitors that induce a structural conformation associated with decreased stability in vitro.

How do covalent EGFR family inhibitors target TRIB2?

We focused our studies on electrophilic type IV kinase (covalent) inhibitors, since they are amenable to comparative chemical and mutational analysis in their targets [31, 70]. We confirmed that at-least two highly conserved TRIB2 Cys residues interact with afatinib [71] in vitro. These Cys-residues are unique within the distorted TRIB2 αC-helix (Fig. 1A). In most canonical kinases, including EGFR family members, helix positioning is critical for catalysis and switching between inactive and active enzyme conformations, both of which are targets for small molecules [72]. Dynamic helix positioning is also important for small molecule interactions, including 'inactive' conformations in kinases in which the αC-helix adapts upon binding, as described for HER2 [73]. The conformation of the flexible C-helix relative to the ATP binding P-loop can also create an allosteric binding pocket in canonical kinases such as ERK1/2, which can be targeted with selective non ATP-competitive inhibitors such as SCH772984 [74]. In TRIB2, the unique disposition of Cys residues (Fig. 1A) makes it vulnerable to destabilization by the covalent inhibitors afatinib, neratininb and osimertinib in vitro. These compounds also undergo a Michael addition to a distinct, but conserved, Cys residue in the ATP-binding site of EGFR-family tyrosine kinases (Cys^{797} in EGFR, Cys^{805} in HER2 and Cys^{803} in HER4) [61]. Afatinib also demonstrates low, but detectable, affinity for the pseudokinase domain of

HER3 [75, 76], which possesses a non-modifiable Ser residue (Ser^{794}) at the equivalent position as Cys^{797} of EGFR, and assumes a pseudo 'active' catalytic conformation, despite possessing exceptionally low kinase activity [76, 77]. At nanomolar concentrations, afatinib is relatively specific for EGFR and HER2 in cells, although at micromolar concentrations other canonical kinases also appear to be targeted [9]. Moreover, osimertinib possesses cross-reactivity with kinases [9] and non-kinases such as lysosomal cathepsins [78]. In the absence of a high-resolution TRIB2 pseudokinase structure, we can only model the conformation(s) relevant for small molecule interaction, although the N-lobe has shared (SLE motif) and distinct (Cys^{96} and Cys^{104}) features compared to TRIB1, TRIB3 and STK40 [15], and TRIB1 adopts at least two conformations, one of which ('SLE-in') appears vulnerable to small molecules [56]. This is confirmed by biochemical differences in the ability of TRIB2 to bind weakly to ATP, which likely predisposes it to C-helix targeting by the kinase inhibitors identified here (fig. S8). None of the EGFR family members possess a Cys residue in the C-helical region conserved in TRIB2, and the overall identity between HER2 and TRIB2 in the (pseudo)kinase domain is very low indeed (~22%). We believe that our discovery of TRIB2 binding to covalent compounds like afatinib owes as much to the availability of reactive Cys residues adjacent to the unique allosteric pocket in the pseudokinase domain, as to their weak affinity for the vestigial ATP-binding site. Our work also builds on previous studies in which pseudokinase domains were targeted with compounds [3], such as TX1-85-1 [8], which covalently binds Cys^{721} in the roof of the ATP site (inducing HER3 degradation in cells) and non-covalent JAK2 JH2 (pseudokinase) domain ligands [79, 80].

In the course of compound screening, we discovered that unrelated classes of ATP-competitive kinase inhibitors, including thienopyrimidines [55] and thiazolylquinazolines [53] also bound to TRIB2 in vitro. In contrast to destabilization (a feature of covalent TRIB2-binding compounds) these compounds stabilize TRIB2, similar to lapatinib and the pyrrolo[3,2-*d*]pyrimidine EGFR-family inhibitor TAK-285, which are known to bind to HER2 in an active-like conformation [81]. Of relevance, lapatinib and TAK-285 did not induce TRIB2 degradation in cells, although CETSA suggested an interaction with lapatinib (fig. S11). Previous studies found that lapatinib can also deprive HER2 of an interaction with the Hsp90-Cdc37 system, leading to time-dependent HER2 degradation at micromolar concentrations [82]. Our data prove that the cellular mechanism by which TRIB2 stability is regulated by compounds is proteasome-based, and we speculate that an afatinib-induced conformational change might induce TRIB2 ubiquitination, or negatively regulate interaction with an unknown stabilizing factor(s), similar to effects of Hsp90 inhibitors on Cdc37 kinome clients [83-85]. Consistently, TRIB2 abundance is regulated by ubiquitination [19, 68, 69], and future work will attempt to correlate TRIB2 small molecule interactions with dynamic changes in ubiqutination status.

The future: Targeting TRIB2 with kinase inhibitors in cancer cells and beyond The finding that TRIB2 stabilizing and destabilizing small molecule compounds can be discovered by DSF profiling is an important advance for the analysis of compounds that target catalytically-deficient pseudokinases, and confirms that TRIB2 represents a *bona fide* pseudokinase drug target [5]. We found that conserved Cys residues in TRIB2 make it vulnerable to families of small molecule kinase inhibitors originally developed as dual nanomolar covalent EGFR and HER2 inhibitors. These residues also represent an additional form of selectivity filter, permitting targeting of TRIB2 by these compounds at micromolar concentrations in cells. Based on this mechanism, a lack of equivalent Cys residues in other pseudokinases, including TRIB1, TRIB3 and STK40, likely precludes interaction with covalent compounds such as afatinib through this mechanism.

Using a chemical genetic approach, we provide evidence that afatinib induces on-target effects through TRIB2 stability and AKT signaling in a variety of human cancer cells. Experimental 'on-target' effects of covalent TRIB2-destablising agents were confirmed using chemical genetics and a mutant TRIB2 allele, similar to 'drug-resistance' approaches developed for compound target validation in the kinase inhibitor field [86-89]. Importantly, drug effects were prevented by mutation of two TRIB2 Cys C-helix residues, confirming a meaningful cellular interaction. Afatinib binding was also validated by DSF, MS, MST and by employing in-cell TSA (CETSA) approaches with exogenous TRIB2. Finally, we established that afatinib (and neratinib) exhibit sub-micromolar toxicity in the human AML model cell line U937, where they are 10-20 fold more effective at cell killing compared to equipotent EGFR-family or EGFR specific inhibitors [72], which do not degrade TRIB2 but still block ERK activation. U937 cells are known to be hypersensitive to TRIB2 siRNA knock-down and to require TRIB2 for cell survival [68].

Conclusions

Our work demonstrates that covalent inhibitors such as afatinib possess TRIB2 degrading-activity in human cells at micromolar concentrations, in similar ranges to those reported for other destabilizing kinase inhibitors, such as the related TRIB2 destabilizing quinazaline neratinib [90]. Although we cannot rule out simultaneous dual effects of afatinib on TRIB2 and ERK/AKT pathways contributing to cellular phenotypes, we provide direct evidence that TRIB2-binding is required for TRIB2 destabilization and AKT regulation. Should an appropriate concentration of drug permit a direct TRIB2 interaction, an 'off-target' TRIB2-dependent phenotype might be relevant to compound efficacy (or side-effects) in patient groups exposed to high concentrations of these covalent compounds. Many severe side effects of drugs are only detected after long-term clinical use, potentially leading to their withdrawal [91], and covalent drugs have the potential to accumulate to relatively high concentrations in cells. Indeed, side-effects of lapatinib [92] and afatinib [93] are already well-established in patients. Based on our mechanistic studies, it will be interesting to develop

ELISA-based procedures to quantify effects of these drugs on TRIB2 protein stability in clinical samples obtained from patients, as part of broader proteomics approaches to establish all the intracellular targets of such compounds. Our study also provides impetus for generating improved (ideally TRIB2-specific) covalent compounds that induce TRIB2 degradation at lower (nanomolar) concentrations, ideally by synthesising compounds in which the effects of eliminating or preserving tyrosine kinase inhibition can be compared side-by-side. In the latter case, simultaneous elimination of TRIB2 and inhibition of the ERK-signaling pathway could be a polypharmacological asset, especially if TRIB2-dependent drug-resistance in tumor cells [39, 50] can be modulated by tyrosine kinase inhibition. Together, our data establish a new paradigm for the pharmacological evaluation of agents that interfere with TRIB2-based signaling and raises the intriguing possibility that clinical inhibitors might be used as TRIB2-degrading agents in research, and possibly clinical, contexts. This information can also be exploited in the future for targeting a variety of TRIB2-overexpressing solid [94, 95] and haematological [21, 68] tumors.

MATERIALS AND METHODS:

Chemicals, reagents, antibodies and TRIB2 small molecule screen

Tetracycline (TET) and doxycycline, MG132, AICAR and chloroquine were purchased from Sigma. Afatinib, neratinib, osimertinib, ibrutinib, erlotinib, lapatinib, TAK-285, BI2536, BI6727, gefitinib and bortezomib were purchased from LC laboratories or Selleck. Total AKT, pSer 473 AKT, pThr 308 AKT, total ERK1/2, dual pThr 202/pTyr 204 ERK1/2, cleaved Caspase 3 and α-tubulin antibodies were purchased from New England Biolabs and employed as previously described [51, 96]. 6His-HRP and α-FLAG antibodies were purchased from Sigma, GAPDH antibody was purchased from Proteintech and a polyclonal rabbit α-TRIB2 antibody was raised towards a unique N-terminal human TRIB2 sequence and affinity purified prior to evaluation with recombinant TRIB2 and a variety of human cellular extracts.

The PKIS chemical library (designated as SB, GSK or GW compounds) comprises 367 ATP-competitive kinase inhibitors, covering ~30 chemotypes (~70% with molecular mass <500 Da and clogP values <5) that were originally designated as ATP-competitive inhibitors of 24 distinct protein kinase targets, including multiple EGFR and HER2 tyrosine kinase classes [52]. Compounds were stored frozen as 10 mM stocks in DMSO. For initial screening, compounds were pre-incubated with TRIB2 for 10 minutes and then employed for DSF, which was initiated by the addition of fluorescent SYPRO Orange. For dose-dependent thermal-shift assays a compound range was prepared by serial dilution in DMSO, and added directly into the assay to the appropriate final concentration, as previously described [97] [Add Byrne BJ papers]. All control experiments contained 2% (v/v) DMSO, which had essentially no effect on TRIB2 stability.

Cloning, Site Directed Mutagenesis and recombinant protein production

pET30 6His-TRIB2 (and various deletion or amino acid substitution constructs, including an N-terminal FLAG-tagged TRIB2, termed His-FLAG-TRIB2), and pET30a 6His-PKAc, which encodes catalytically-active cAMP-dependent protein kinase domain, have been described previously [40, 49]. Full length TRIB2 was also cloned into pOPINJ to generate a His-GST-TRIB2 encoding construct for Glutathione-*S*-transferase (GST) pull-down assays. MCL-1 and A-1210477 were prepared as described [61]. TRIB1 (84-372) was a kind gift from Dr. Peter Mace, and was purified as described previously for TRIB2 [40]. Briefly, protein expression was induced in BL21(DE3) pLysS bacteria with 0.4 mM IPTG, and after overnight culture at 18°C, proteins were purified to near homogeneity using an initial affinity step (immobilised metal affinity chromatography (IMAC) or glutathione-sepharose chromatography) followed by size exclusion chromatography (16/600 Superdex 200) in appropriate buffers. S473D 6His-AKT1 (DU1850, amino acids 118-470), either active (PDK1-phosphorylated to a specific activity of 489 U/mg) or inactive, were purchased from the DSTT

(University of Dundee), and stored at -80°C prior to analysis. Site directed mutagenesis was performed as previously described [98], using KOD Hot Start DNA polymerase (Millipore) and appropriate mutagenic primer pairs (sourced from IDT). All plasmids were Sanger-sequenced across the entire coding regions to confirm expected codon usage.

Differential Scanning Fluorimetry (DSF)

Thermal-shift assays were performed using an Applied Biosystems StepOnePlus Real-Time PCR instrument using a standard DSF procedure previously developed and validated for the analysis of kinases [47, 49] and pseudokinases [48]. All proteins were diluted in 20 mM Tris/HCl (pH 7.4), 100 mM NaCl and 1 mM DTT to a concentration of 5 μM and then incubated with the indicated concentration of compound in a total reaction volume of 25 μL, with final concentration of 2% (v/v) DMSO. SYPRO Orange (Invitrogen) was used as a fluoresecence probe. The temperature was raised in regular 0.3 °C intervals from 25°C to 95°C. Compound binding experiments were assessed in duplicate and then reported relative to DMSO controls.

Mass Spectrometry analysis of TRIB2 afatinib binding

To evaluate TRIB2 binding in vitro, afatinib was incubated for 15 min with purified 6His-TRIB2 at a 1:10 molar ratio, then denatured with 0.05 % (w/v) RapiGest SF (Waters, UK) and digested with chymotrypsin (1:20 protease:protein (w/w) ratio) for 16 h at 25 °C. RapiGest hydrolysis was induced by the addition of triflouroacetic acid (TFA) to 1 % (v/v), incubated at 37 °C for 1h. Insoluble product was removed by centrifugation (13, 000 x g, 20 min). Reversed-phase HPLC separation was performed using an UltiMate 3000 nano system (Dionex) coupled in-line with a Thermo Orbitrap Fusion Tribrid mass spectrometer (Thermo Scientific, Bremen, Germany). 500 fmol digested peptides were loaded onto the trapping column (PepMap100, C18, 300 μm × 5 mm), using partial loop injection, for 7 min at a flow rate of 9 μL/min with 2% (v/v) MeCN, 0.1% (v/v) TFA and then resolved on an analytical column (Easy-Spray C18 75 μm × 500 mm, 2 μm bead diameter column) using a gradient of 96.2% A (0.1% (v/v) formic acid (FA)): 3.8% B (80% (v/v) MeCN, 0.1% (v/v) FA) to 50% B over 35 min at a flow rate of 300 nL/min. MS1 spectra were acquired over *m/z* 400 – 1500 in the orbitrap (60 K resolution at 200 *m/z*). Data-dependent MS2 analysis was performed using a top speed approach (cycle time of 3 s), using higher-energy collisional dissociation (HCD) and electron-transfer and higher-energy collision dissociation (EThcD) for fragmentation, with product ions being detected in the ion trap (rapid mode). Data were processed using Thermo Proteome Discoverer (v. 1.4) and spectra were searched in MASCOT against the *E. coli* IPI database with the added sequence of full-length 6His-TRIB2 (1-343). Parameters were set as follows: MS1 tolerance of 10 ppm, MS/MS mass tolerance of 0.6 Da, oxidation of methionine and afatanib binding at cysteine as variable modifications. MS2 spectra were interrogated manually.

To evaluate the interaction between afatinib and intact TRIB2 protein, TRIB2 was incubated with afatinib as above, and then desalted using a C4 desalting trap (Waters MassPREP™ Micro desalting column, 2.1 × 5 mm, 20 µ m particle size, 1000 Å pore size). TRIB2 was eluted with 50 % (v/v) MeCN, 0.1 % (v/v) formic acid. Intact TRIB2 mass analysis was performed using a Waters nano ACQUITY Ultra Performance liquid chromatography (UPLC) system coupled to a Waters SYNAPT G2. Samples were eluted from a C4 trap column at a flow rate of 10 µL/min using three repeated 0-100 % acetonitrile gradients. Data was collected between 400 and 3500 *m/z* and processed using MaxEnt1 (maximum entropy software, Waters Corporation).

TRIB2 modeling and compound docking

The structure model of human TRIB2 pseudokinase domain [13] (UniProt ID: Q92519) (residues 58-308) was built with MODELLER [99] using a crystal structure of TRIB1 pseudokinase in the open 'SLE-in' conformation [56] as a template. The homology model was subjected to energy minimization using the Rosetta Relax protocol [100]. The chemical structures of afatinib (CID 10184653) and neratinib (CID 9915743) were retrieved from PubChem. Afatanib and neratinib were docked to our TRIB2 model using AutoDock Vina [62] with an exhaustiveness of 100, rigid body, and a search space centered on Cys^{96}. Top poses were identified where the enamide group localizes near the Cys^{96} sulfhydryl moiety. For comparison, we employed a crystal structure of EGFR in complex with afatinib (PDB: 4g5j). Missing disordered loop regions in the structure were modelled using RosettaRemodel [101] with default settings. The covalently-bound afatinib was removed from the structure and allowed to re-dock with AutoDock Vina using the same parameters from TRIB2, with the exception of search space being centered on EGFR Cys^{797}. Top poses were identified where the enamide group localized near the Cys^{797} sulfhydryl moeity. For molecular dynamics simulations, TRIB2 and EGFR binding modes were parameterized with GROMACS 5.1.3. Afatinib and neratinib were parameterized with GAFF [102] using ACPYPE [103]. Protein was fixed with AMBER99SB-ILDN force field and solvated with TIP3P water model in a dodecahedron box at least 1 nm larger than the protein in all directions. Sodium and chloride ions were added to neutralize the system. Neighbor lists for non-bonded interactions were maintained by the Verlet cutoff scheme and long-range electrostatics were calculated by the Particle Mesh Ewald method. Energy minimization was performed with steepest descent followed by conjugate gradient until the total energy was under 100 kJ/mol/nm. The system was heated from 0 to 310 K, then pressurized to 1 bar. Position restraint was applied to non-hydrogen atoms during equilibration. The production run was performed in 2 fs time-steps. Data visualization was performed in VMD and PyMOL.

MicroScale Thermophoresis

A Monolith NT.115 instrument (NanoTemper Technologies GmbH) was employed for MST analysis.

His-TRIB2 was initially labelled with a NanoTemper labelling kit; the fluorescent red dye NT-647 was coupled via NHS chemistry to the N-terminal His-tag, placing the fluorophore away from the pseudokinase domain. For MST, the reaction was performed in 20 mM Bicine pH 9.0, 100 mM NaCl, 5% glycerol, 0.05% Tween-20 and 2 % (v/v) DMSO. Fluorescent TRIB2 (~5 μM) was kept constant in the assay, while final afatinib and TAK-285 concentration was titrated over a 3 nM and 50-100 μM range. Near-saturation binding was achieved, allowing for an affinity to be estimated for the reversible interaction between afatinib, TAK-285 and fluorescent TRIB2. NT-647-linked MCL-1 and A-1210477 was employed as a positive control.

Cell lines and reagents

Flp-In T-REx parental HeLa cells (Invitrogen) were cultured in DMEM with 4 mM L-glutamine, 10 % (v/v) Foetal Bovine Serum (FBS), Penicillin and Streptomycin (Gibco) as described [86]. To engineer Tetracycline (TET)-controlled expression of FLAG-tagged full length TRIB2 in human Flp-In T-REx cell lines, the host plasmid pcDNA5/FRT/TO, encoding full length TRIB2 sequences (or appropriate amino acid substitution(s)), with a single N-terminal FLAG tag (1 μg DNA per well in a 6 well plate of cells) were co-transfected with 9 μg of pOG44 Flp-Recombinase Expression Vector using lipofectamine. Cells that had successfully integrated the FLAG-tagged TRIB2 sequence were stably selected with 200 μg/mL Hygromycin B, according to the manufacturer's instructions. TET was added at a final concentration of 1 μg/ml to medium in order to induce FLAG-TRIB2 expression. For transient transfection, 50% confluent HeLa cells were transfected with 40 μg DNA per 10 cm dish for 48 h prior to lysis.

For serum starvation, stable HeLa cells were grown until ~60% confluent in complete medium (+FBS), washed with PBS, and replaced with serum-free DMEM for 16 h. Cells were then incubated with DMEM containing 10% (v/v) FBS ± 1 μg/ml TET for 16 h, followed by addition of appropriate inhibitor for 4h. All whole cell lysates were generated with modified RIPA buffer (see below). Non-adherent AML-derived human U937 cells (which express high levels of endogenous TRIB2 protein) were supplied by Dr Karen Keeshan, University of Glasgow and were cultured as previously described [21].

MTT cytotoxicity assay

U937 cells were seeded in a 96 well plate at a concentration of 0.2 x 10^6 cells/mL, 18 hours prior to compound addition, which was performed in triplicate, with all experiments including a final concentration of 0.1% DMSO (v/v). To quantify U937 cell viability, metabolic activity was assessed 72 h after compound exposure using an MTT assay (Abcam), as described previously [104]. Briefly, Thiazolyl blue tetrazolium bromide was dissolved in PBS and added to cells at a final concentration of 0.25 mg/mL and incubated at 37 °C for 3 hours. The reaction was stopped by the addition of 50 μL

of acidified 10% SDS, followed by reading of absorbance at 570 nm. Viability was defined relative to DMSO-containing controls incubated for the same period of time.

Immunoblotting and CETSA

HeLa and U937 whole cell lysates were generated using a modified RIPA buffer (50 mM Tris–HCl pH 7.4, 1 % (v/v) NP-40, 1 % (v/v) SDS, 100 mM NaCl, 100 nM Okadaic acid) supplemented with protease and phosphatase inhibitors (Roche), and brief sonication. For western blotting, samples were boiled for 5 min in sample buffer (50 mM Tris pH 6.8, 1% SDS, 10% glycerol, 0.01% Bromophenol Blue, 10 mM DTT). Subsequently, and between 40 and 120 μg of total protein was resolved by SDS–PAGE followed by transfer onto nitrocellulose membrane (BioRad). After blocking in pH TBS-T + 5% milk, pH 7.4), primary and secondary antibodies were incubated in the same condition, and proteins were detected using HRP-conjugated antibodies and ECL reagent. Immunoblots were quantified using ImageJ software, as previously described [96]. For lambda phosphatase treatment, 40 μg FLAG-TRIB2 expressing stable cell extracts in lysis buffer without SDS and phosphatase inhibitors were incubated with 10 ng of purified λ-phosphatase for 30 min at 37°C prior to processing for western blotting.

For in-cell CETSA we employed a previously published procedure [105]. Briefly, stable HeLa cells were incubated with TET for 16h to induce expression of FLAG-TRIB2, and at ~90% confluency, were incubated with 0.1% (v/v) DMSO or 100 μM of the indicated compound for 1h. Intact cells were isolated by trypsinization (1 min) and resuspended in PBS, and then aliquoted into individual PCR tubes prior to heating at the indicated temperature in a PCR thermal cycler for 3 min. Cells were then placed on ice for 2 min and lysed by sonication, prior to centrifugation at 16,000 x g for 20 minutes at 4°C. The soluble lysate was analysed for the presence of FLAG-TRIB2 and α-tubulin by immunoblotting.

Statistical analysis

All experimental procedures were repeated in at least 3 separate experiments with matched positive and negative controls (unless stated otherwise). Results are expressed as mean ± SD for all in vitro experiments and data are expressed as the mean ± standard deviation. When applied, statistical significance of differences (*P ≤0.05) was assessed using a Students t-test for normally-distributed data. All statistical tests were performed using Prism 7 (GraphPad Software)

SUPPLEMENTARY MATERIALS:

Fig. S1. Discovery of multiple PKIS compounds as TRIB2-binding compounds.

Fig. S2. Chemical structure of pre-clinical and clinical compounds evaluated in this study.

REFERENCES AND NOTES:

1. Eyers, P.A. and J.M. Murphy, *Dawn of the dead: protein pseudokinases signal new adventures in cell biology.* Biochemical Society transactions, 2013. **41**(4): p. 969-74.
2. Kung, J.E. and N. Jura, *Structural Basis for the Non-catalytic Functions of Protein Kinases.* Structure, 2016. **24**(1): p. 7-24.
3. Byrne, D.P., D.M. Foulkes, and P.A. Eyers, *Pseudokinases: update on their functions and evaluation as new drug targets.* Future medicinal chemistry, 2017. **9**(2): p. 245-265.
4. Reiterer, V., P.A. Eyers, and H. Farhan, *Day of the dead: pseudokinases and pseudophosphatases in physiology and disease.* Trends in cell biology, 2014. **24**(9): p. 489-505.
5. Foulkes, D.M., et al., *Tribbles pseudokinases: novel targets for chemical biology and drug discovery?* Biochemical Society transactions, 2015. **43**(5): p. 1095-103.
6. Hari, S.B., E.A. Merritt, and D.J. Maly, *Conformation-selective ATP-competitive inhibitors control regulatory interactions and noncatalytic functions of mitogen-activated protein kinases.* Chemistry & biology, 2014. **21**(5): p. 628-35.
7. Jones, L.H., *Small-Molecule Kinase Downregulators.* Cell chemical biology, 2018. **25**(1): p. 30-35.
8. Xie, T., et al., *Pharmacological targeting of the pseudokinase Her3.* Nature chemical biology, 2014. **10**(12): p. 1006-12.
9. Klaeger, S., et al., *The target landscape of clinical kinase drugs.* Science, 2017. **358**(6367).
10. Zhang, J., P.L. Yang, and N.S. Gray, *Targeting cancer with small molecule kinase inhibitors.* Nature reviews. Cancer, 2009. **9**(1): p. 28-39.
11. Ferguson, F.M. and N.S. Gray, *Kinase inhibitors: the road ahead.* Nature reviews. Drug discovery, 2018.
12. Bailey, F.P., et al., *Going for broke: targeting the human cancer pseudokinome.* The Biochemical journal, 2015. **465**(2): p. 195-211.
13. Eyers, P.A., K. Keeshan, and N. Kannan, *Tribbles in the 21st Century: The Evolving Roles of Tribbles Pseudokinases in Biology and Disease.* Trends in cell biology, 2017. **27**(4): p. 284-298.
14. Otsuki, L. and A.H. Brand, *Cell cycle heterogeneity directs the timing of neural stem cell activation from quiescence.* Science, 2018. **360**(6384): p. 99-102.
15. Murphy, J.M., et al., *Molecular Mechanism of CCAAT-Enhancer Binding Protein Recruitment by the TRIB1 Pseudokinase.* Structure, 2015. **23**(11): p. 2111-21.
16. Eyers, P.A., *TRIBBLES: A Twist in the Pseudokinase Tail.* Structure, 2015. **23**(11): p. 1974-6.
17. Durzynska, I., et al., *STK40 Is a Pseudokinase that Binds the E3 Ubiquitin Ligase COP1.* Structure, 2017. **25**(2): p. 287-294.
18. Keeshan, K., et al., *Transformation by Tribbles homolog 2 (Trib2) requires both the Trib2 kinase domain and COP1 binding.* Blood, 2010. **116**(23): p. 4948-57.
19. Liang, K.L., et al., *Human TRIB2 Oscillates during the Cell Cycle and Promotes Ubiquitination and Degradation of CDC25C.* International journal of molecular sciences, 2016. **17**(9).
20. Salome, M., J. Campos, and K. Keeshan, *TRIB2 and the ubiquitin proteasome system in cancer.* Biochemical Society transactions, 2015. **43**(5): p. 1089-94.
21. O'Connor, C., et al., *The presence of C/EBPalpha and its degradation are both required for TRIB2-mediated leukaemia.* Oncogene, 2016. **35**(40): p. 5272-5281.
22. Cromm, P.M. and C.M. Crews, *Targeted Protein Degradation: from Chemical Biology to Drug Discovery.* Cell chemical biology, 2017. **24**(9): p. 1181-1190.
23. Lai, A.C. and C.M. Crews, *Induced protein degradation: an emerging drug discovery paradigm.* Nature reviews. Drug discovery, 2017. **16**(2): p. 101-114.
24. Ostrem, J.M., et al., *K-Ras(G12C) inhibitors allosterically control GTP affinity and effector interactions.* Nature, 2013. **503**(7477): p. 548-51.
25. Lim, S.M., et al., *Therapeutic targeting of oncogenic K-Ras by a covalent catalytic site inhibitor.* Angewandte Chemie, 2014. **53**(1): p. 199-204.

26. Corcoran, A. and T.G. Cotter, *Redox regulation of protein kinases.* The FEBS journal, 2013. **280**(9): p. 1944-65.
27. Chaikuad, A., et al., *The Cysteinome of Protein Kinases as a Target in Drug Development.* Angewandte Chemie, 2018. **57**(16): p. 4372-4385.
28. Liu, Q., et al., *Developing irreversible inhibitors of the protein kinase cysteinome.* Chemistry & biology, 2013. **20**(2): p. 146-59.
29. Zhao, Z., et al., *Determining Cysteines Available for Covalent Inhibition Across the Human Kinome.* Journal of medicinal chemistry, 2017. **60**(7): p. 2879-2889.
30. Hatcher, J.M., et al., *SRPKIN-1: A Covalent SRPK1/2 Inhibitor that Potently Converts VEGF from Pro-angiogenic to Anti-angiogenic Isoform.* Cell chemical biology, 2018.
31. Zhang, T., et al., *Covalent targeting of remote cysteine residues to develop CDK12 and CDK13 inhibitors.* Nature chemical biology, 2016. **12**(10): p. 876-84.
32. Du, K., et al., *TRB3: a tribbles homolog that inhibits Akt/PKB activation by insulin in liver.* Science, 2003. **300**(5625): p. 1574-7.
33. Zanella, F., et al., *Human TRIB2 is a repressor of FOXO that contributes to the malignant phenotype of melanoma cells.* Oncogene, 2010. **29**(20): p. 2973-82.
34. Liang, K.L., L. Rishi, and K. Keeshan, *Tribbles in acute leukemia.* Blood, 2013. **121**(21): p. 4265-70.
35. Keeshan, K., et al., *Tribbles homolog 2 inactivates C/EBPalpha and causes acute myelogenous leukemia.* Cancer cell, 2006. **10**(5): p. 401-11.
36. Salazar, M., et al., *TRIB3 suppresses tumorigenesis by controlling mTORC2/AKT/FOXO signaling.* Molecular & cellular oncology, 2015. **2**(3): p. e980134.
37. Salazar, M., et al., *Loss of Tribbles pseudokinase-3 promotes Akt-driven tumorigenesis via FOXO inactivation.* Cell death and differentiation, 2015. **22**(1): p. 131-44.
38. Naiki, T., et al., *TRB2, a mouse Tribbles ortholog, suppresses adipocyte differentiation by inhibiting AKT and C/EBPbeta.* The Journal of biological chemistry, 2007. **282**(33): p. 24075-82.
39. O'Connor, C., et al., *Trib2 expression in granulocyte-monocyte progenitors drives a highly drug resistant acute myeloid leukaemia linked to elevated Bcl2.* Oncotarget, 2018. **9**(19): p. 14977-14992.
40. Bailey, F.P., et al., *The Tribbles 2 (TRB2) pseudokinase binds to ATP and autophosphorylates in a metal-independent manner.* The Biochemical journal, 2015. **467**(1): p. 47-62.
41. de Azambuja, E., et al., *Lapatinib with trastuzumab for HER2-positive early breast cancer (NeoALTTO): survival outcomes of a randomised, open-label, multicentre, phase 3 trial and their association with pathological complete response.* The Lancet. Oncology, 2014. **15**(10): p. 1137-46.
42. Singh, M. and H.R. Jadhav, *Targeting non-small cell lung cancer with small-molecule EGFR tyrosine kinase inhibitors.* Drug discovery today, 2018. **23**(3): p. 745-753.
43. Kosaka, T., et al., *Response Heterogeneity of EGFR and HER2 Exon 20 Insertions to Covalent EGFR and HER2 Inhibitors.* Cancer research, 2017. **77**(10): p. 2712-2721.
44. Sequist, L.V., et al., *Neratinib, an irreversible pan-ErbB receptor tyrosine kinase inhibitor: results of a phase II trial in patients with advanced non-small-cell lung cancer.* Journal of clinical oncology : official journal of the American Society of Clinical Oncology, 2010. **28**(18): p. 3076-83.
45. Bose, P. and H. Ozer, *Neratinib: an oral, irreversible dual EGFR/HER2 inhibitor for breast and non-small cell lung cancer.* Expert opinion on investigational drugs, 2009. **18**(11): p. 1735-51.
46. Murphy, J.M., P.D. Mace, and P.A. Eyers, *Live and let die: insights into pseudoenzyme mechanisms from structure.* Current opinion in structural biology, 2017. **47**: p. 95-104.
47. Rudolf, A.F., et al., *A comparison of protein kinases inhibitor screening methods using both enzymatic activity and binding affinity determination.* PloS one, 2014. **9**(6): p. e98800.
48. Murphy, J.M., et al., *A robust methodology to subclassify pseudokinases based on their nucleotide-binding properties.* The Biochemical journal, 2014. **457**(2): p. 323-34.

49. Byrne, D.P., et al., *cAMP-dependent protein kinase (PKA) complexes probed by complementary differential scanning fluorimetry and ion mobility-mass spectrometry.* The Biochemical journal, 2016. **473**(19): p. 3159-75.
50. Hill, R., et al., *TRIB2 confers resistance to anti-cancer therapy by activating the serine/threonine protein kinase AKT.* Nature communications, 2017. **8**: p. 14687.
51. Bago, R., et al., *The hVps34-SGK3 pathway alleviates sustained PI3K/Akt inhibition by stimulating mTORC1 and tumour growth.* The EMBO journal, 2016. **35**(17): p. 1902-22.
52. Elkins, J.M., et al., *Comprehensive characterization of the Published Kinase Inhibitor Set.* Nature biotechnology, 2016. **34**(1): p. 95-103.
53. Waterson, A.G., et al., *Alkynyl pyrimidines as dual EGFR/ErbB2 kinase inhibitors.* Bioorganic & medicinal chemistry letters, 2006. **16**(9): p. 2419-22.
54. Gaul, M.D., et al., *Discovery and biological evaluation of potent dual ErbB-2/EGFR tyrosine kinase inhibitors: 6-thiazolylquinazolines.* Bioorganic & medicinal chemistry letters, 2003. **13**(4): p. 637-40.
55. Rheault, T.R., et al., *Thienopyrimidine-based dual EGFR/ErbB-2 inhibitors.* Bioorganic & medicinal chemistry letters, 2009. **19**(3): p. 817-20.
56. Jamieson, S.A., et al., *Substrate binding allosterically relieves autoinhibition of the TRIB1 pseudokinase.* Science signaling, 2018. **Submitted**.
57. Solca, F., et al., *Target binding properties and cellular activity of afatinib (BIBW 2992), an irreversible ErbB family blocker.* The Journal of pharmacology and experimental therapeutics, 2012. **343**(2): p. 342-50.
58. Roy, A., A. Kucukural, and Y. Zhang, *I-TASSER: a unified platform for automated protein structure and function prediction.* Nature protocols, 2010. **5**(4): p. 725-38.
59. Vucetic, S., et al., *Flavors of protein disorder.* Proteins, 2003. **52**(4): p. 573-84.
60. Jerabek-Willemsen, M., et al., *Molecular interaction studies using microscale thermophoresis.* Assay and drug development technologies, 2011. **9**(4): p. 342-53.
61. Milani, M., et al., *DRP-1 is required for BH3 mimetic-mediated mitochondrial fragmentation and apoptosis.* Cell death & disease, 2017. **8**(1): p. e2552.
62. Miller, R.M., et al., *Electrophilic fragment-based design of reversible covalent kinase inhibitors.* Journal of the American Chemical Society, 2013. **135**(14): p. 5298-301.
63. Schwartz, P.A., et al., *Covalent EGFR inhibitor analysis reveals importance of reversible interactions to potency and mechanisms of drug resistance.* Proceedings of the National Academy of Sciences of the United States of America, 2014. **111**(1): p. 173-8.
64. Trott, O. and A.J. Olson, *AutoDock Vina: improving the speed and accuracy of docking with a new scoring function, efficient optimization, and multithreading.* Journal of computational chemistry, 2010. **31**(2): p. 455-61.
65. Bianco, G., et al., *Covalent docking using autodock: Two-point attractor and flexible side chain methods.* Protein science : a publication of the Protein Society, 2016. **25**(1): p. 295-301.
66. Northrop, B.H. and R.N. Coffey, *Thiol-ene click chemistry: computational and kinetic analysis of the influence of alkene functionality.* Journal of the American Chemical Society, 2012. **134**(33): p. 13804-17.
67. Martinez Molina, D., et al., *Monitoring drug target engagement in cells and tissues using the cellular thermal shift assay.* Science, 2013. **341**(6141): p. 84-7.
68. Rishi, L., et al., *Regulation of Trib2 by an E2F1-C/EBPalpha feedback loop in AML cell proliferation.* Blood, 2014. **123**(15): p. 2389-400.
69. Qiao, Y., Y. Zhang, and J. Wang, *Ubiquitin E3 ligase SCF(beta-TRCP) regulates TRIB2 stability in liver cancer cells.* Biochemical and biophysical research communications, 2013. **441**(3): p. 555-9.
70. Gao, Y., et al., *Overcoming Resistance to the THZ Series of Covalent Transcriptional CDK Inhibitors.* Cell chemical biology, 2018. **25**(2): p. 135-142 e5.
71. Modjtahedi, H., et al., *A comprehensive review of the preclinical efficacy profile of the ErbB family blocker afatinib in cancer.* Naunyn-Schmiedeberg's archives of pharmacology, 2014. **387**(6): p. 505-21.
72. Wodicka, L.M., et al., *Activation state-dependent binding of small molecule kinase inhibitors: structural insights from biochemistry.* Chemistry & biology, 2010. **17**(11): p. 1241-9.

73. Aertgeerts, K., et al., *Structural analysis of the mechanism of inhibition and allosteric activation of the kinase domain of HER2 protein.* The Journal of biological chemistry, 2011. **286**(21): p. 18756-65.
74. Chaikuad, A., et al., *A unique inhibitor binding site in ERK1/2 is associated with slow binding kinetics.* Nature chemical biology, 2014. **10**(10): p. 853-60.
75. Davis, M.I., et al., *Comprehensive analysis of kinase inhibitor selectivity.* Nature biotechnology, 2011. **29**(11): p. 1046-51.
76. Jura, N., et al., *Structural analysis of the catalytically inactive kinase domain of the human EGF receptor 3.* Proceedings of the National Academy of Sciences of the United States of America, 2009. **106**(51): p. 21608-13.
77. Shi, F., et al., *ErbB3/HER3 intracellular domain is competent to bind ATP and catalyze autophosphorylation.* Proceedings of the National Academy of Sciences of the United States of America, 2010. **107**(17): p. 7692-7.
78. Niessen, S., et al., *Proteome-wide Map of Targets of T790M-EGFR-Directed Covalent Inhibitors.* Cell chemical biology, 2017. **24**(11): p. 1388-1400 e7.
79. Newton, A.S., et al., *JAK2 JH2 Fluorescence Polarization Assay and Crystal Structures for Complexes with Three Small Molecules.* ACS medicinal chemistry letters, 2017. **8**(6): p. 614-617.
80. Puleo, D.E., et al., *Identification and Characterization of JAK2 Pseudokinase Domain Small Molecule Binders.* ACS medicinal chemistry letters, 2017. **8**(6): p. 618-621.
81. Linhardt, R.J., et al., *Structure and activity of a unique heparin-derived hexasaccharide.* The Journal of biological chemistry, 1986. **261**(31): p. 14448-54.
82. Polier, S., et al., *ATP-competitive inhibitors block protein kinase recruitment to the Hsp90-Cdc37 system.* Nature chemical biology, 2013. **9**(5): p. 307-12.
83. Schneider, C., et al., *Pharmacologic shifting of a balance between protein refolding and degradation mediated by Hsp90.* Proceedings of the National Academy of Sciences of the United States of America, 1996. **93**(25): p. 14536-41.
84. Taipale, M., et al., *Chaperones as thermodynamic sensors of drug-target interactions reveal kinase inhibitor specificities in living cells.* Nature biotechnology, 2013. **31**(7): p. 630-7.
85. Taipale, M., et al., *Quantitative analysis of HSP90-client interactions reveals principles of substrate recognition.* Cell, 2012. **150**(5): p. 987-1001.
86. Scutt, P.J., et al., *Discovery and exploitation of inhibitor-resistant aurora and polo kinase mutants for the analysis of mitotic networks.* The Journal of biological chemistry, 2009. **284**(23): p. 15880-93.
87. Sloane, D.A., et al., *Drug-resistant aurora A mutants for cellular target validation of the small molecule kinase inhibitors MLN8054 and MLN8237.* ACS chemical biology, 2010. **5**(6): p. 563-76.
88. Eyers, P.A., et al., *Use of a drug-resistant mutant of stress-activated protein kinase 2a/p38 to validate the in vivo specificity of SB 203580.* FEBS letters, 1999. **451**(2): p. 191-6.
89. Zhang, T., et al., *Discovery of potent and selective covalent inhibitors of JNK.* Chemistry & biology, 2012. **19**(1): p. 140-54.
90. Zhang, Y., et al., *Neratinib induces ErbB2 ubiquitylation and endocytic degradation via HSP90 dissociation in breast cancer cells.* Cancer letters, 2016. **382**(2): p. 176-185.
91. Uetrecht, J. and D.J. Naisbitt, *Idiosyncratic adverse drug reactions: current concepts.* Pharmacological reviews, 2013. **65**(2): p. 779-808.
92. Moy, B. and P.E. Goss, *Lapatinib-associated toxicity and practical management recommendations.* The oncologist, 2007. **12**(7): p. 756-65.
93. Yap, T.A., et al., *Phase I trial of the irreversible EGFR and HER2 kinase inhibitor BIBW 2992 in patients with advanced solid tumors.* Journal of clinical oncology : official journal of the American Society of Clinical Oncology, 2010. **28**(25): p. 3965-72.
94. Hill, R., et al., *TRIB2 as a biomarker for diagnosis and progression of melanoma.* Carcinogenesis, 2015. **36**(4): p. 469-77.
95. Grandinetti, K.B., et al., *Overexpression of TRIB2 in human lung cancers contributes to tumorigenesis through downregulation of C/EBPalpha.* Oncogene, 2011. **30**(30): p. 3328-35.

96. Tyler, R.K., et al., *Phosphoregulation of human Mps1 kinase.* The Biochemical journal, 2009. **417**(1): p. 173-81.
97. Byrne, D.P., et al., *New tools for evaluating protein tyrosine sulphation: Tyrosyl Protein Sulphotransferases (TPSTs) are novel targets for RAF protein kinase inhibitors.* The Biochemical journal, 2018.
98. McSkimming, D.I., et al., *KinView: a visual comparative sequence analysis tool for integrated kinome research.* Molecular bioSystems, 2016. **12**(12): p. 3651-3665.
99. Webb, B. and A. Sali, *Protein Structure Modeling with MODELLER.* Methods in molecular biology, 2017. **1654**: p. 39-54.
100. Nivon, L.G., R. Moretti, and D. Baker, *A Pareto-optimal refinement method for protein design scaffolds.* PloS one, 2013. **8**(4): p. e59004.
101. Huang, P.S., et al., *RosettaRemodel: a generalized framework for flexible backbone protein design.* PloS one, 2011. **6**(8): p. e24109.
102. Wang, J., et al., *Development and testing of a general amber force field.* Journal of computational chemistry, 2004. **25**(9): p. 1157-74.
103. Sousa da Silva, A.W. and W.F. Vranken, *ACPYPE - AnteChamber PYthon Parser interfacE.* BMC research notes, 2012. **5**: p. 367.
104. Bailey, F.P., et al., *Kinome-wide transcriptional profiling of uveal melanoma reveals new vulnerabilities to targeted therapeutics.* Pigment cell & melanoma research, 2018. **31**(2): p. 253-266.
105. Savitski, M.M., et al., *Tracking cancer drugs in living cells by thermal profiling of the proteome.* Science, 2014. **346**(6205): p. 1255784.

ACKNOWLEDGEMENTS:

The authors acknowledge Dr Peter Mace, University of Otago, NZ, for the gift of TRIB1 (84-372) plasmid. We also thank Sam Evans for excellent technical support, including media preparation.

FUNDING:

This work was funded by two BBSRC DTP studentships (to DMF and SF), a Tools and Resources Development Fund award (BB/N021703/1) to PAE, Royal Society Research Grants (to PAE and CEE), and North West Cancer Research grants (to PAE, CR1088 and CR1097). Funding for NK from the National Institutes of Health (5RO1GM114409) is also acknowledged. The SGC is a registered charity (number 1097737) that receives funds from AbbVie, Bayer Pharma AG, Boehringer Ingelheim, Canada Foundation for Innovation, Eshelman Institute for Innovation, Genome Canada, Innovative Medicines Initiative (EU/EFPIA) [ULTRA-DD grant no. 115766], Janssen, Merck KGaA Darmstadt Germany, MSD, Novartis Pharma AG, Ontario Ministry of Economic Development and Innovation, Pfizer, São Paulo Research Foundation-FAPESP, Takeda, and The Wellcome Trust [106169/ZZ14/Z].

AUTHOR CONTRIBUTIONS:

PAE obtained funding and designed experiments alongside DMF, DPB, FPB, SF and CEE. KK provided critical reagents and experimental advice. SS, WY and NK conducted TRIB2 modeling and compound docking. PAE generated the TRIB2 antibody, SF and CEE provided MS expertise; CW,

DHD and WJZ provided the PKIS library, screening advice and additional medicinal chemistry. PAE wrote the paper, with contributions from all the authors, who approved the final version.

COMPETING INTERESTS:

There are no perceived conflicts of interest from any authors. The SGC receives direct funds from a variety of pharmaceutical companies (see above), although it remains entirely independent.

DATA AND MATERIALS AVAILABILITY:

Original TRIB2 PKIS screening data is presented in table S1. Further compound information can be obtained by contacting DHD or WJZ. All data needed to evaluate conclusions made are available in the main or supplementary sections of the paper.

FIGURE LEGENDS:

Fig. 1. Full-length TRIB2 is a target for protein kinase inhibitors in vitro

(A) Top, sequence alignment of human TRIB2, TRIB1, TRIB3, and STK40/SgK495, highlighting Cys-rich residues (numbered in red) in the TRIB2 pseudokinase domain. Bottom, blot of the recombinant proteins employed for *in vitro* analysis. 5 μg of the indicated purified proteins were resolved by SDS-PAGE. WT, wild-type. **(B)** Thermal denaturation profiles of recombinant proteins. A representative unfolding profile is shown. T_m values (±SD) were obtained from 3 separate fluorescence profiling experiments, each point assayed in duplicate. **(C)** The ability of GST-TRIB2 to interact with active (PDK1-phosphorylated) or inactive (non PDK1-phosphorylated) S473D AKT1 was assessed by GSH-sepharose pull-down followed by immunoblotting. PDK1 phosphorylated S473D AKT is phosphorylated on Thr^{308} (right panel), but binds much more weakly to TRIB2. 'Master-mix' input is shown,left. **(D)** Transient transfection of TET-inducible FLAG-TRIB2 leads to increased AKT phosphorylation on Ser^{473}. **(E)** TRIB2 DSF screen using PKIS. 5 μM His-TRIB2 was used for all DSF analysis. ΔT_m values were calculated for each compound (N=2). Scattergraph of data highlights a wide variety of compounds that either stabilize or destabilize TRIB2 in vitro. Cut off values of > + 3.5 °C and < - 2°C were used to designate 'hits'. **(F)** Comparative DSF analysis of clinical and preclinical kinase inhibitors as potential TRIB2-binding compounds. LAP=lapatinib, TAK=TAK-285, AFA=afatinib, NER=neratinib, OSI=osimertinib, IBR=ibrutinib, ERL=erlotinib, GEF=gefitinib. **(G)** Dose-dependent analysis of thermal shifts induced by clinical TRIB2-binding compounds. Compounds were tested at 5, 10, 20, 40, 80 and 160 μM. **(H)** Profiling of TRIB2 and C104Y with selected inhibitors by DSF.

Fig. 2. TRIB2 thermal stability is modulated through Cys binding to covalent inhibitors

(A) Top, schematic cartoon of TRIB2 with domain boundaries numbered and cysteine residues highlighted (red). (Bottom) SDS-PAGE of 5 μg recombinant TRIB2 proteins. **(B)** Thermal denaturation profiles of 5 μM WT-TRIB2 (amino acids 1-343), three truncated variants and an AQLAA triple-point mutant. Representative curves for each protein and average T_m values (±SD) are shown, calculated from N=3 experiments. **(C)** Thermal shift analysis of TRIB2 deletion and AQLAA proteins measured in the presence of a panel of compounds (20 μM). The change in T_m value (ΔT_m) is reported from N=3 experiments, each performed in triplicate, and the chemical structures of each compound are shown for comparison. AFA=afatinib, NER=neratinib, LAP= lapatinib, ERL=erlotinib. **(D)** Thermal denaturation profiles for purified TRIB2 and C96S, C104S and C96/104S proteins. **(E)** Thermal shift analysis of TRIB2 Cys-mutated proteins measured in the presence of a panel of compounds (20 μM). The change in T_m value (ΔT_m) is reported from N=3 experiments.

Fig. 3: Afatinib promotes rapid degradation of FLAG-TRIB2 in an inducible HeLa model

(A) Uninduced (-TET) or Tetracycline-induced (+TET) HeLa cells containing a stably integrated FLAG-TRIB2 transgene were serum starved for 16 hours prior to the addition of serum and lysed at the indicated times. Whole cell extracts were blotted with FLAG antibody to detect FLAG-TRIB2, pSer 473 AKT. Total AKT and total GAPDH served as loading controls. **(B)** A selection of clinically approved kinase inhibitors, including dual EGFR and HER2 and EGFR-specific compounds, were added to TET-induced cells at a final concentration of 10 μM. Stable cells were induced to express FLAG-tagged TRIB2 with tetracycline for 16 hours prior to inhibitor treatment for 4 hours. AFA=afatinib, NER=neratinib, OSI=osimertinib, IBR=ibrutinib, LAP=lapatinib, ERL=erlotinib, GEF=gefitinib. Whole cell extracts were immunoblotted with FLAG, phosphorylated ERK (pERK 1/2), total ERK or GAPDH antibodies. **(C)** Stable HeLa cells were incubated with TET for 16 hours, and then incubated with DMSO (top panels) or 10 μM afatinib (AFA, bottom panels) prior to lysis at the indicated time. 1-hour and 16-hour samples were pre-treated with lambda protein-phosphatase (λPP) prior to SDS-PAGE. Whole cell extracts were immunoblotted with FLAG or GAPDH antibodies. Blots are representative of 3 independent experiments.

Fig. 4. 'On-target' degradation of TRIB2 by afatinib: C96/104S TRIB2 double point mutant is resistant to degradation

(A) The indicated concentration of afatinib, lapatinib or TAK-285 was incubated for 4 hours with isogenic stable HeLa cells expressing FLAG-tagged WT-TRIB2, C96S or C96/104S TRIB2 (induced by TET exposure for 16 hours). After lysis, whole cell extracts were immunblotted with the indicated antibodies. Right, FLAG-TRIB2 abundance was quantified after exposure to 10, 15 and 20 μM afatinib relative to DMSO controls using ImageJ densitometry software. Data are means ± S.D. from N=3 independent biological replicates. **(B)** WT and C96/104S stable HeLa cell lines were subjected to serum block-and-release protocol in the presence (+TET) or absence (-TET) of tetracycline. Subsequently, the indicated compounds (10 μM) were added for 4 hours prior to cell lysis and immunoblotting with the indicated antibodies. AFA=afatinib, ERL=erlotinib. **(C)** FLAG-tagged TRIB2 expressing HeLa cells were incubated with (0.1% v/v) DMSO or afatinib (10 μM), in the presence or absence of MG132 (10 μM for 4 hours, left) or at the indicated time points (right) prior to lysis and processing for immunoblotting. **(D)** Left, FLAG-TRIB2 expressing stable cells were incubated with the indicated concentration of MG132 in the presence or absence of 10 μM afatinib (AFA) for 4 hours prior to cell lysis and immunoblotting. Right, FLAG-TRIB2 expressing stable cells were incubated for 1 hour with MG132 (10 μM), bortezomib (BOR; 10 μM), AICAR (AIC; 1 mM) or Chloroquine (CLQ; 50 μM) prior to the addition of AFA (10 μM) for an additional 4 hours followed

by lysis and immunoblotting with the indicated antibodies. Blots are representative of 3 independent experiments.

Fig. 5. Afatinib rapidly destabilizes endogenous TRIB2 and specifically induces caspase-3 cleavage and U937 cytotoxicity

(A) Endogenous TRIB2 is destabilized in human U937 cells in a dose-dependent manner after a 4-hour exposure to AFA. Cells were incubated with either 0.1% (v/v) DMSO, the indicated concentrations of afatinib, or lapatinib (LAP; 10 μM), erlotinib (ERL; 10 μM) or of the proteasome inhibitor bortezomib (BOR; 10 μM) for 4 hours prior to lysis and immunoblotting of endogenous TRIB2, pERK or cleaved caspase 3. GAPDH served as a loading control. **(B)** Endogenous TRIB2 is destabilized after exposure to afatinib for 24 hours, concomitant with reduced AKT phosphorylation at Ser^{473}. After cell collection and lysis, whole cell extracts were immunoblotted with the indicated antibodies. AKT and GAPDH served as loading controls; ERL and BOR were used at 10 μM. **(C)** The cytotoxicity of a panel of TRIB2-destabilsing small molecules (afatinib, AFA; neratinib, NER) were compared to EGFR inhibitors or the TRIB2 stabilizer TAK-285 (TAK). MTT assays were performed after 72 hours' compound exposure, with bortezomib (BOR) used as a positive control. IC_{50} values (nM, mean ± SD) are derived from N=3 independent experiments, each performed in triplicate. Statistical analysis confirmed a significant difference in cytotoxicity between AFA and ERL (students t-test p value = 0.0104) BOR and ERL (p value = 0.0072) and NER and ERL (p value = 0.0104). Blots are representative of 3 independent experiments.

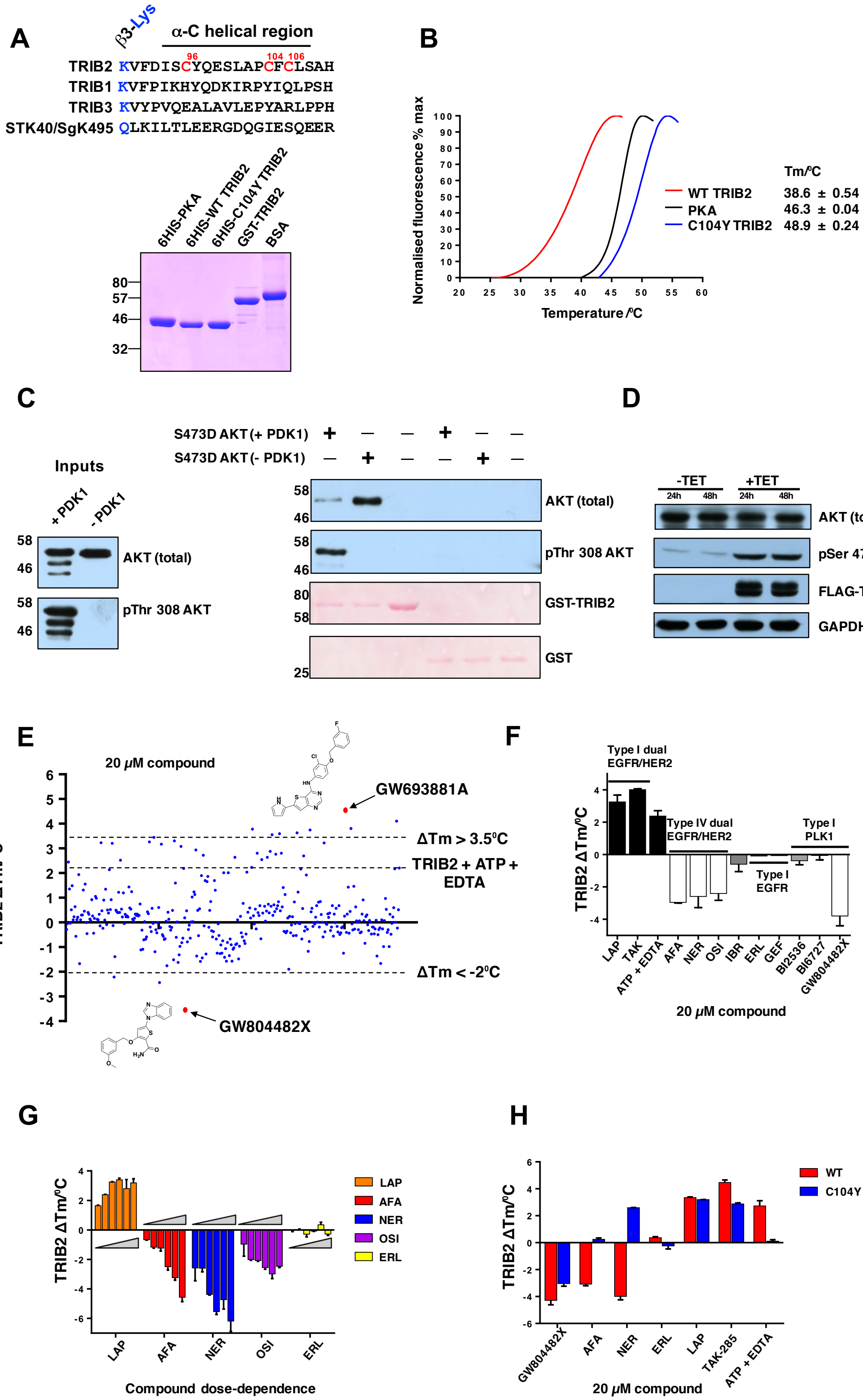
A
β3-Lys
α-C helical region
96
104 106
TRIB2 KVFDISCYQESLAPCFCLSAH
TRIB1 KVFPIKHYQDKIRPYIQLPSH
TRIB3 KVYPVQEALAVLEPYARLPPH
STK40/SgK495 QLKILTLEERGDQGIESQEER
6HIS-PKA
6HIS-WT TRIB2
6HIS-C104Y TRIB2
GST-TRIB2
BSA
80
57
46
32
B
Normalised fluorescence % max
Temperature /°C
Tm/°C
WT TRIB2 38.6 ± 0.54
PKA 46.3 ± 0.04
C104Y TRIB2 48.9 ± 0.24
C
Inputs
+PDK1
-PDK1
AKT (total)
pThr 308 AKT
S473D AKT (+ PDK1)
S473D AKT (- PDK1)
GST-TRIB2
GST
D
-TET
+TET
24h
48h
AKT (total)
pSer 473 AKT
FLAG-TRIB2
GAPDH
E
20 μM compound
GW693881A
ΔTm > 3.5°C
TRIB2 + ATP + EDTA
ΔTm < -2°C
GW804482X
TRIB2 ΔTm/°C
F
Type I dual EGFR/HER2
Type IV dual EGFR/HER2
Type I PLK1
Type I EGFR
LAP
TAK
ATP + EDTA
AFA
NER
OSI
IBR
ERL
GEF
BI2536
BI6727
GW804482X
20 μM compound
G
LAP
AFA
NER
OSI
ERL
Compound dose-dependence
H
WT
C104Y
20 μM compound

Figure 1

A

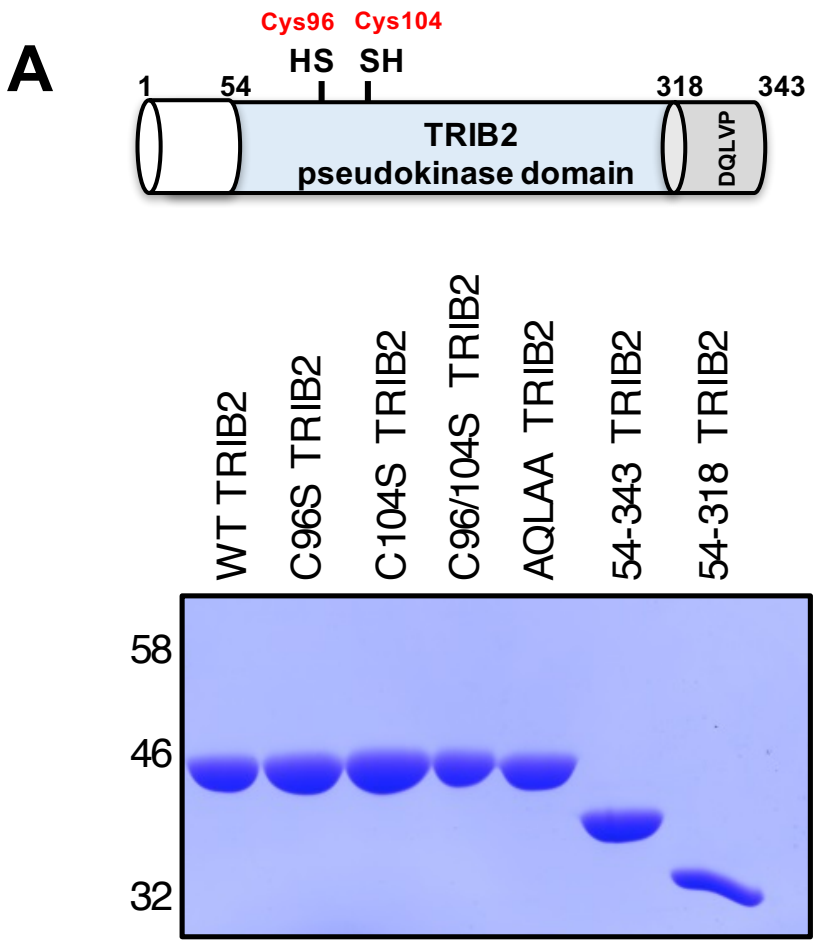

B

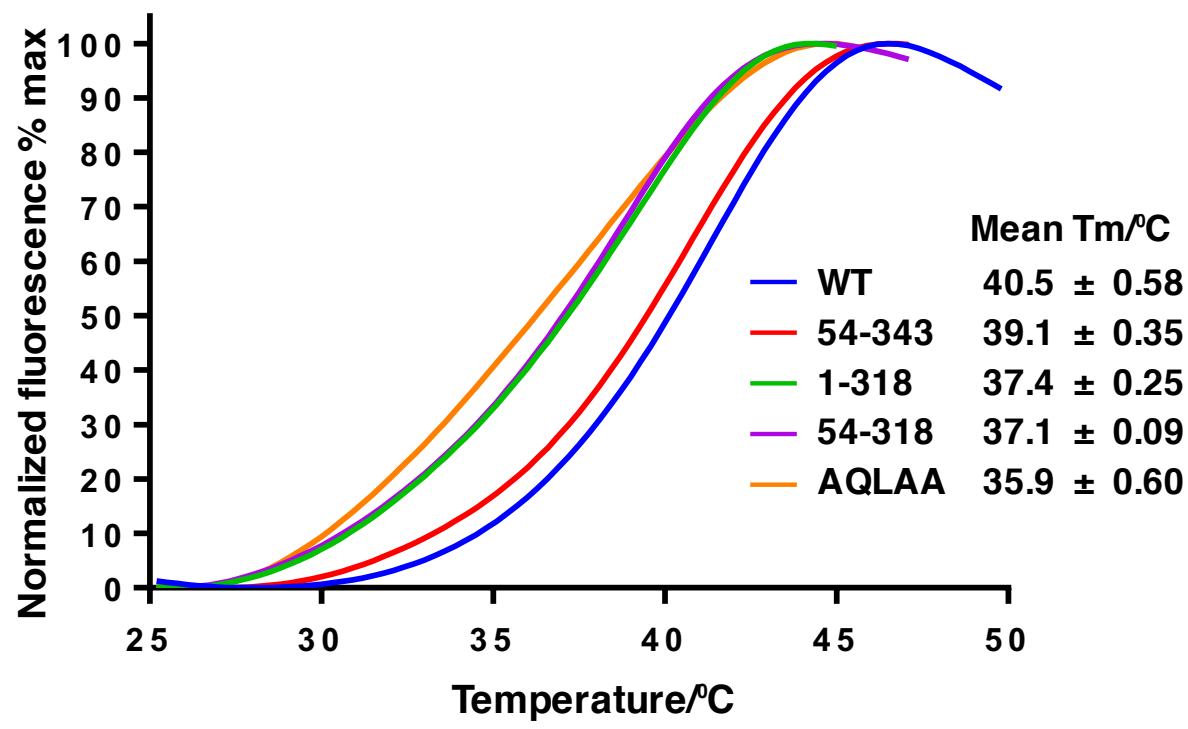

C

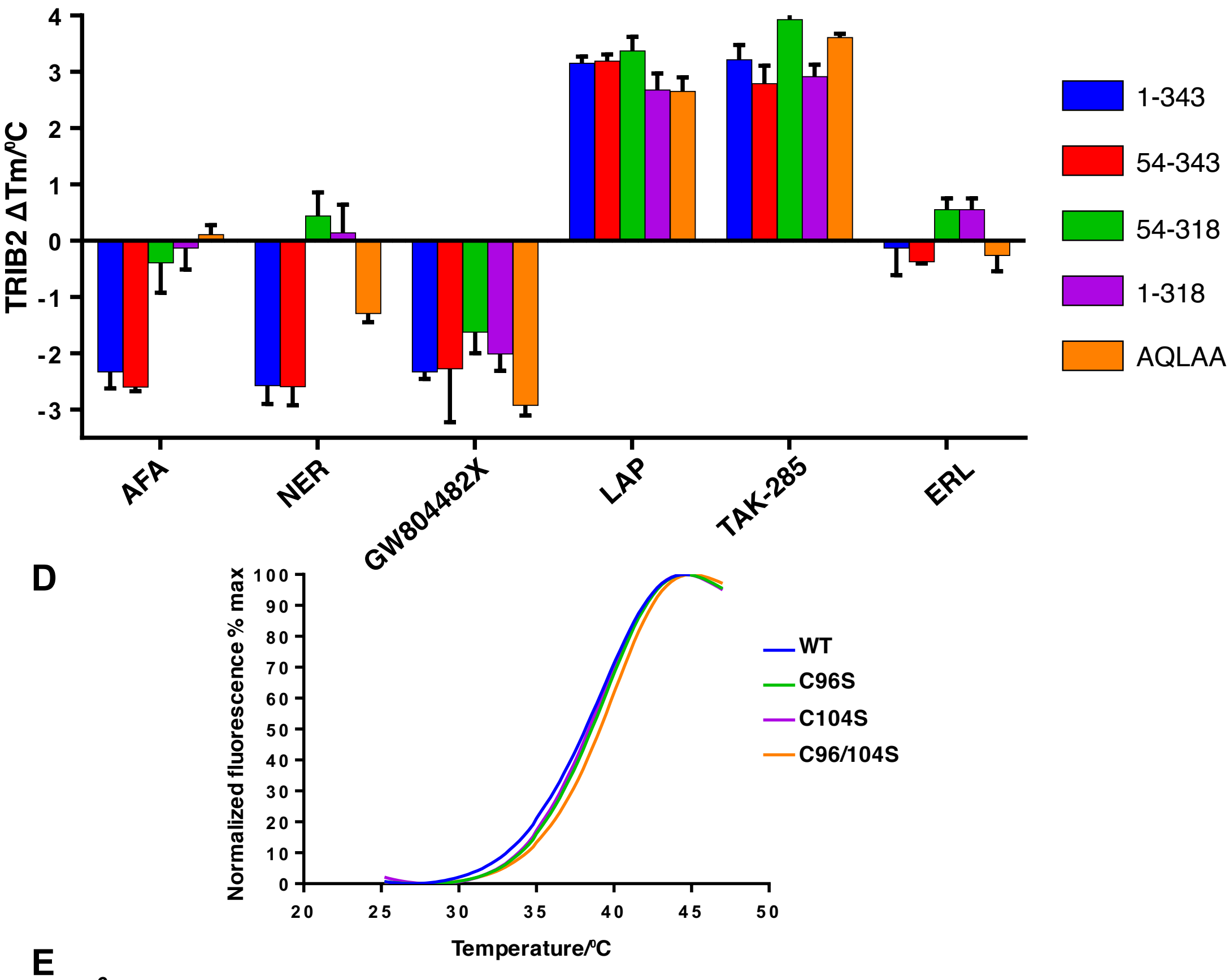

D

E

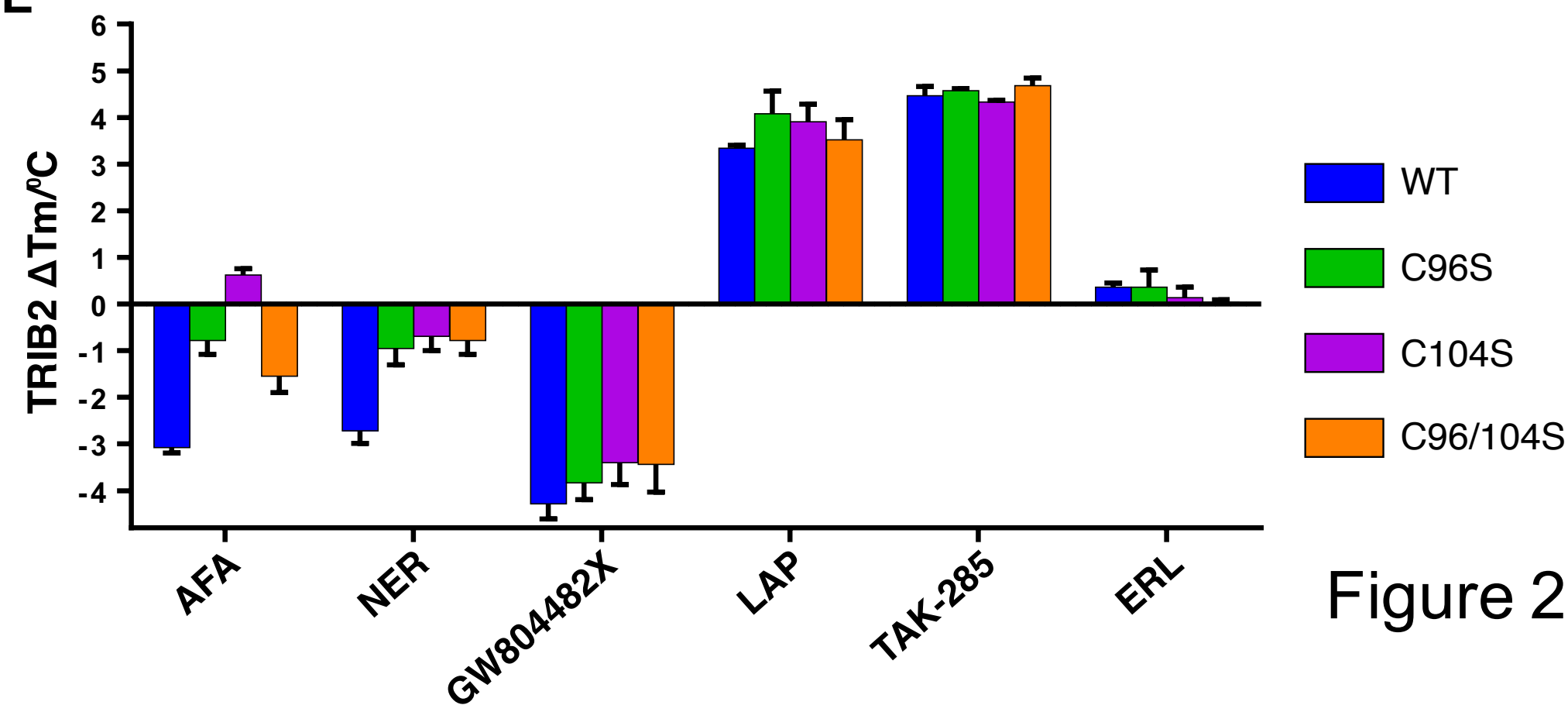

Figure 2

A

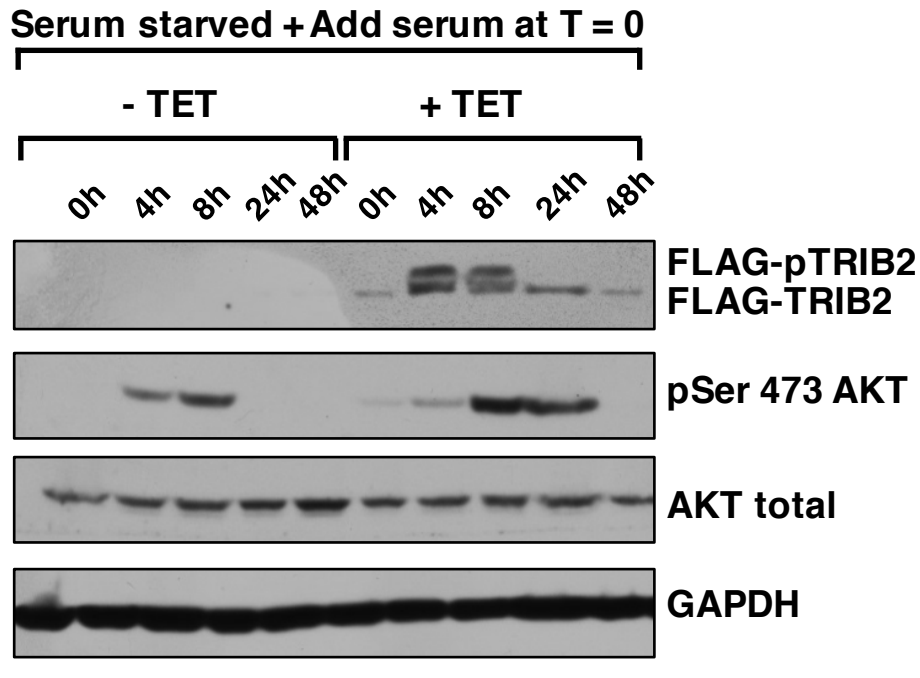
Serum starved + Add serum at T = 0
- TET
+ TET
0h
4h
8h
24h
48h
0h
4h
8h
24h
48h
FLAG-pTRIB2
FLAG-TRIB2
pSer 473 AKT
AKT total
GAPDH

B

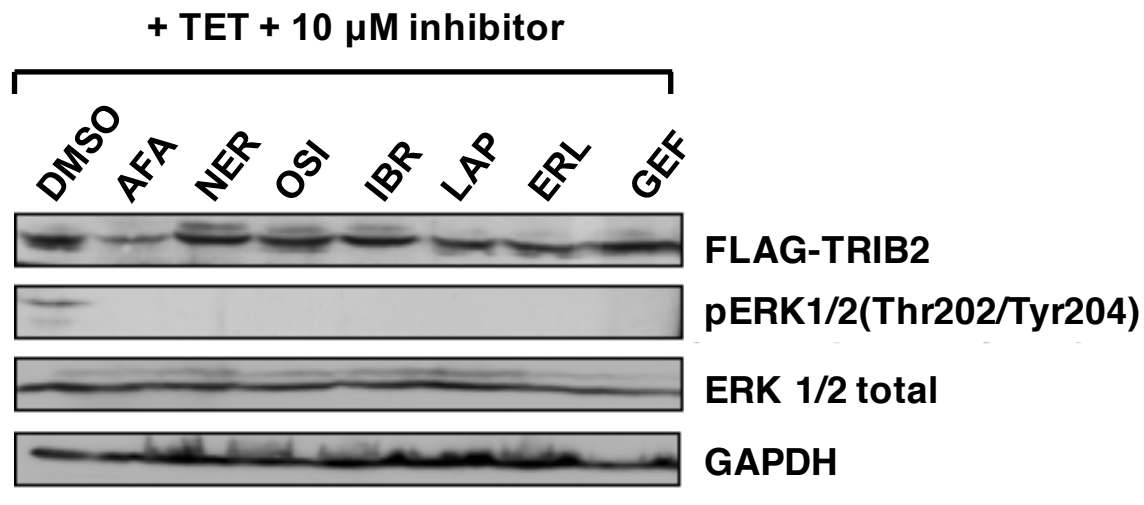
+ TET + 10 μM inhibitor
DMSO
AFA
NER
OSI
IBR
LAP
ERL
GEF
FLAG-TRIB2
pERK1/2(Thr202/Tyr204)
ERK 1/2 total
GAPDH

C

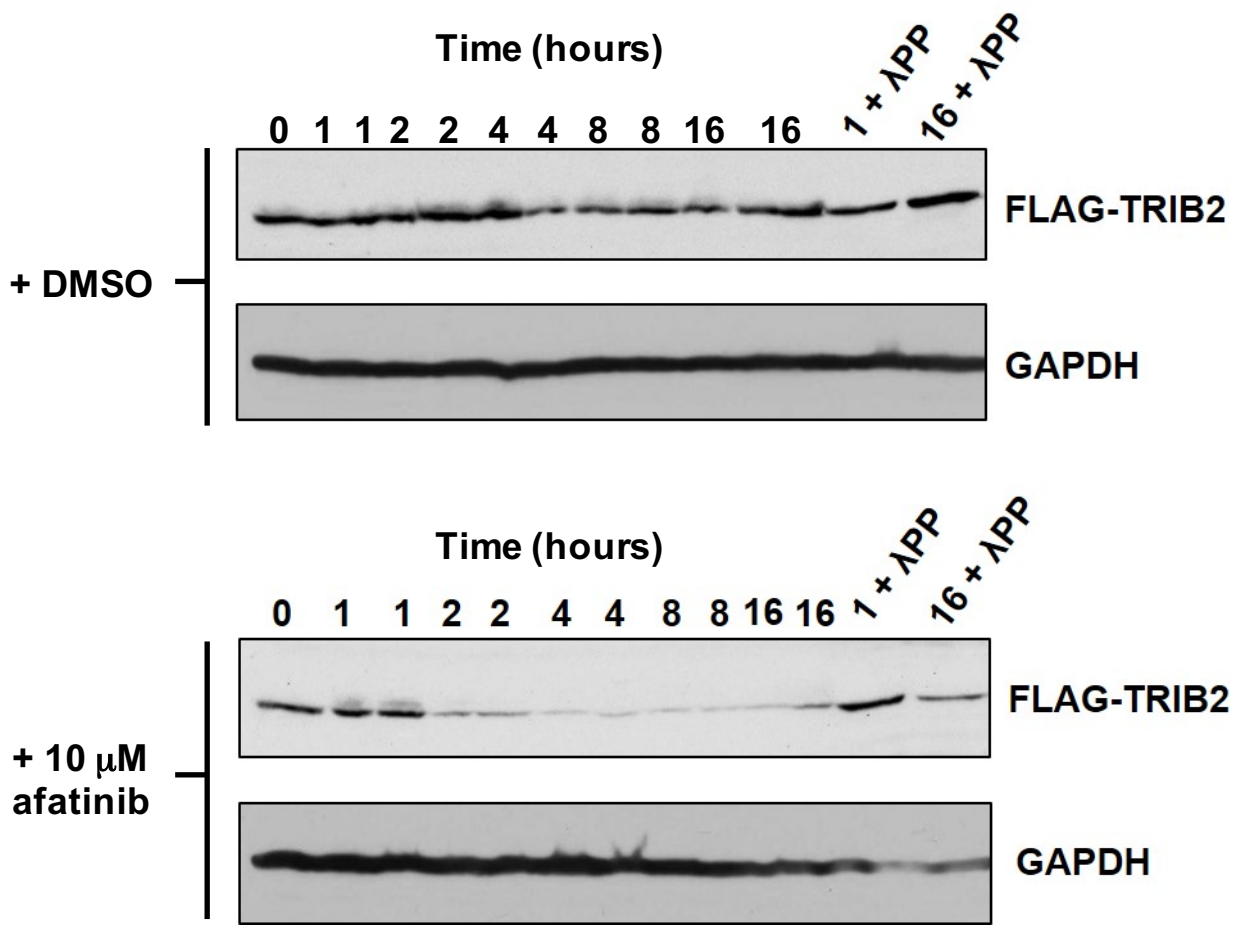
Time (hours)
0 1 1 2 2 4 4 8 8 16 16
1 + λPP
16 + λPP
+ DMSO
FLAG-TRIB2
GAPDH
Time (hours)
0 1 1 2 2 4 4 8 8 16 16
1 + λPP
16 + λPP
+ 10 μM afatinib
FLAG-TRIB2
GAPDH

Figure 3

A

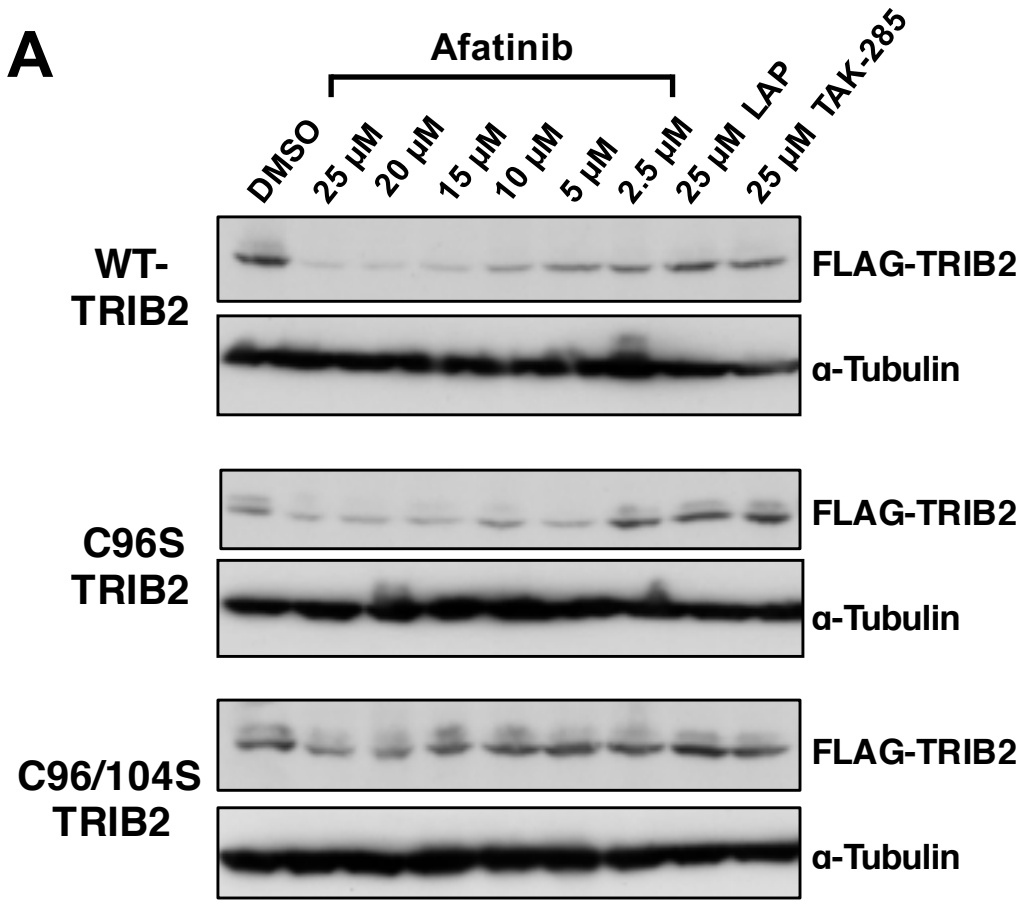

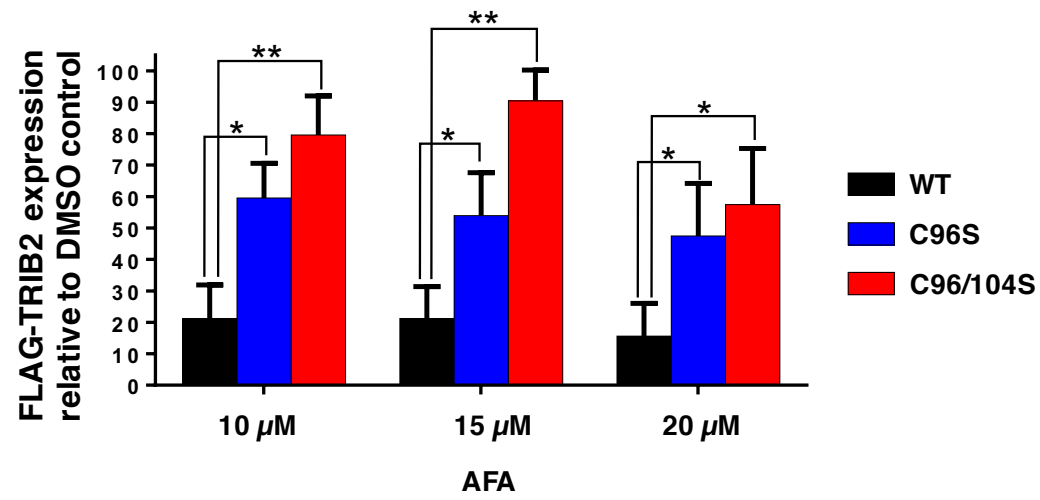

B

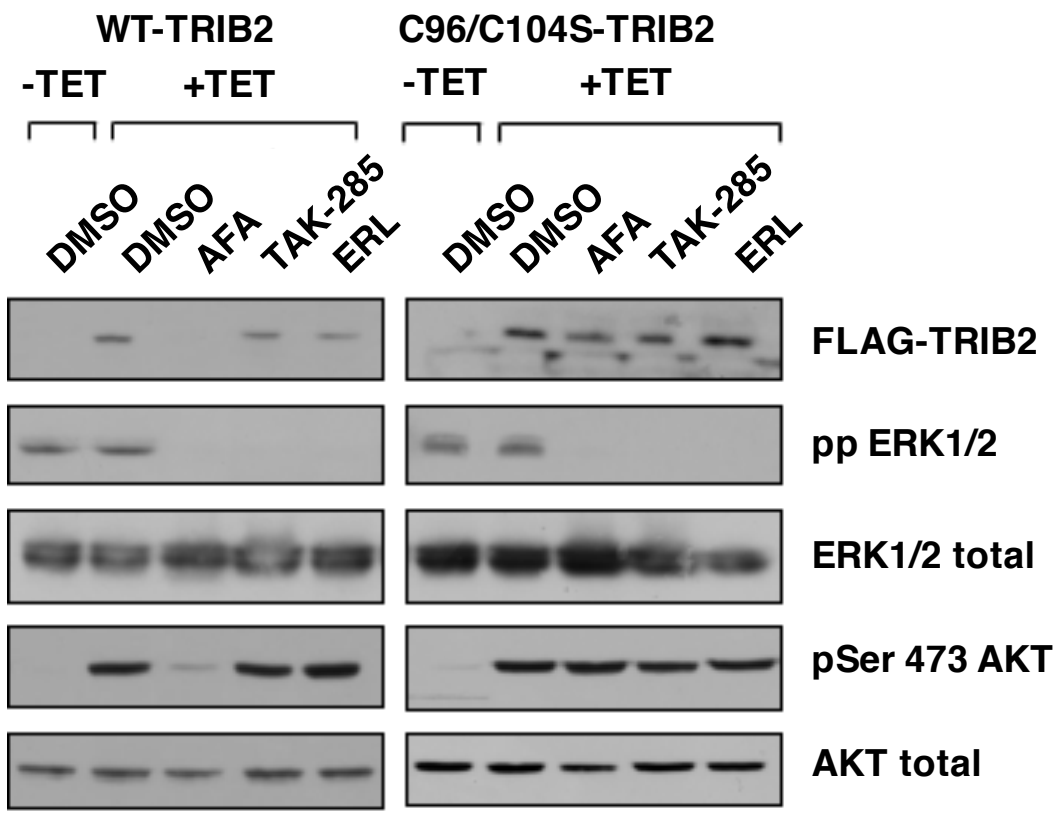

C

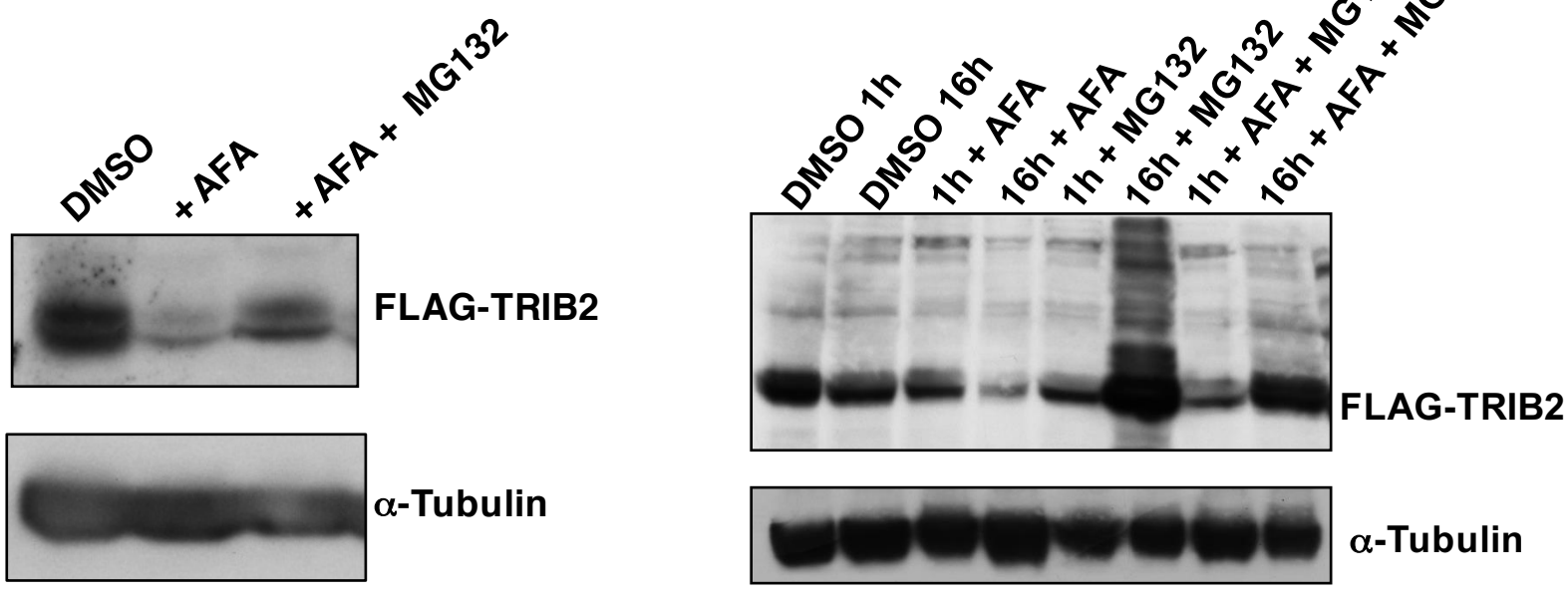

D

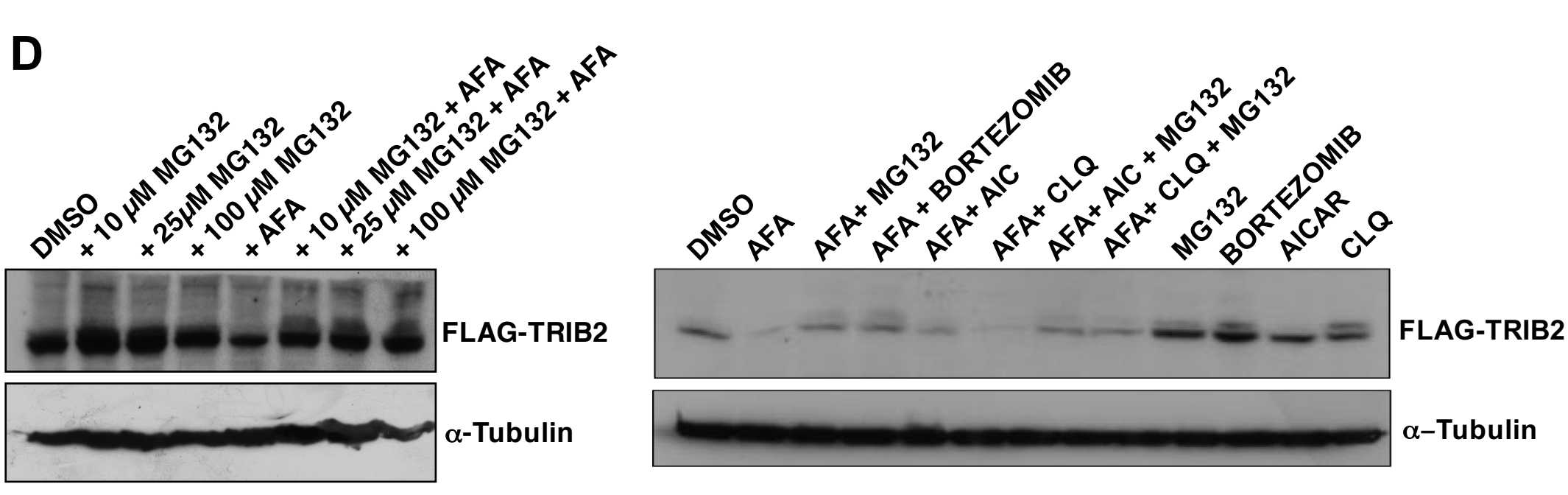

Figure 4

A

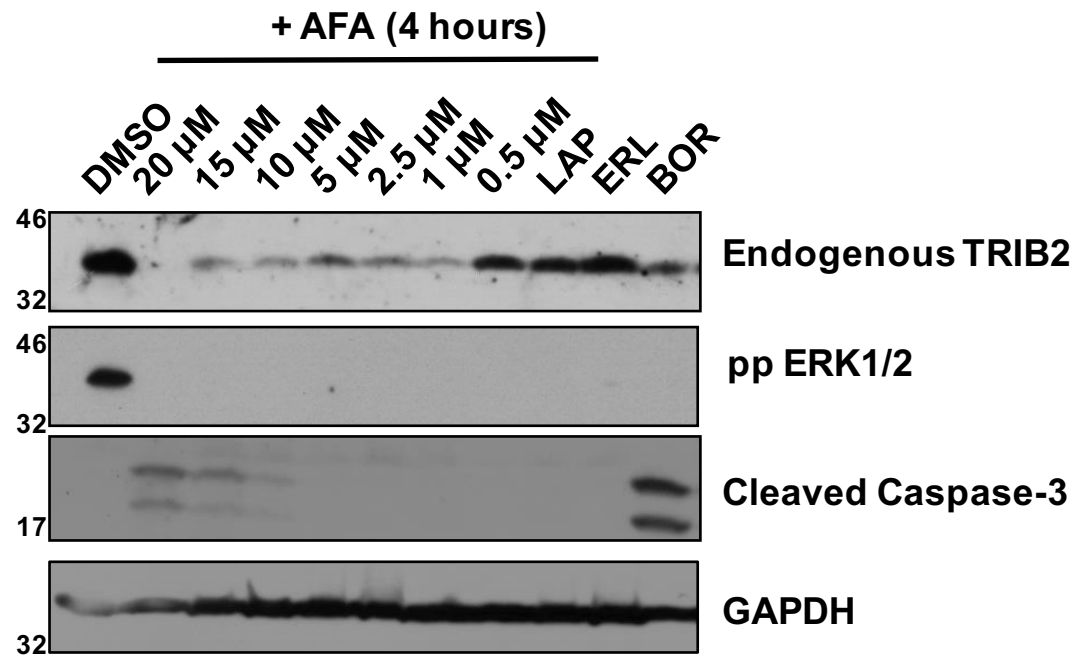
+ AFA (4 hours)
DMSO
20 μM
15 μM
10 μM
5 μM
2.5 μM
1 μM
0.5 μM
LAP
ERL
BOR
46
32
Endogenous TRIB2
46
32
pp ERK1/2
17
Cleaved Caspase-3
32
GAPDH

B

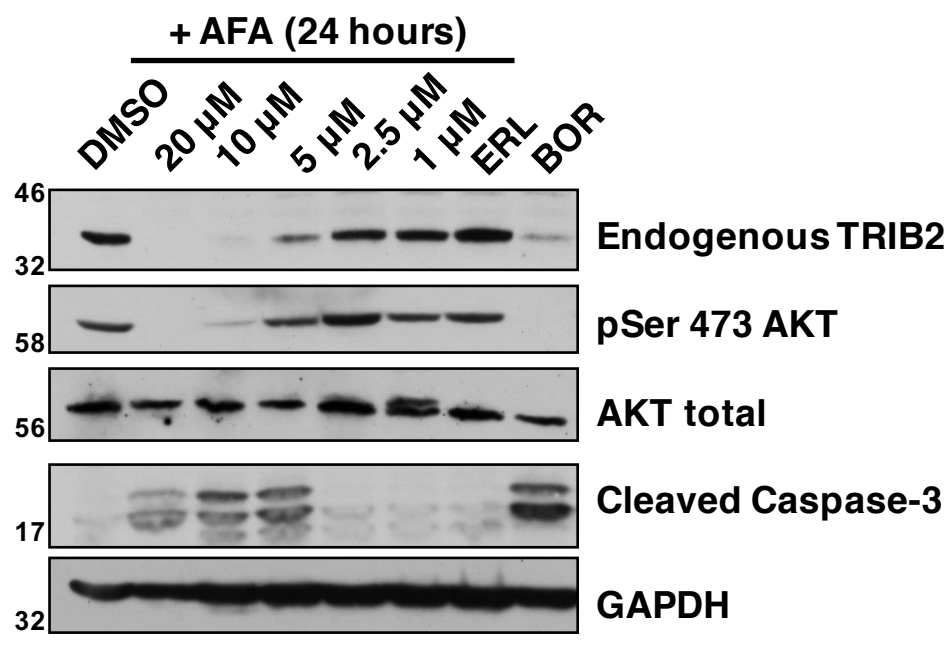
+ AFA (24 hours)
DMSO
20 μM
10 μM
5 μM
2.5 μM
1 μM
ERL
BOR
46
32
Endogenous TRIB2
58
pSer 473 AKT
56
AKT total
17
Cleaved Caspase-3
32
GAPDH

C

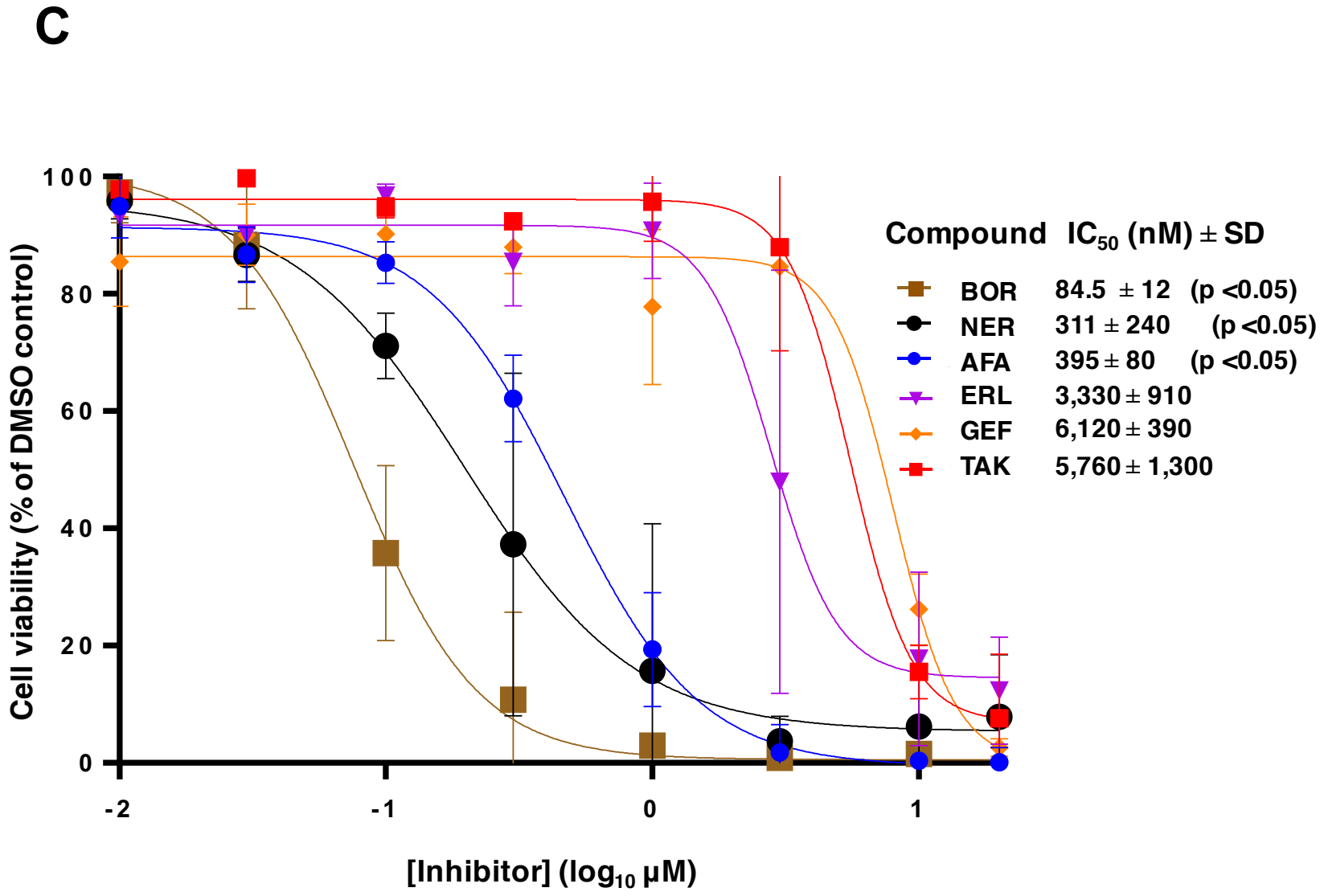
Cell viability (% of DMSO control)
100
80
60
40
20
0
-2
-1
0
1
[Inhibitor] (log10 μM)
Compound IC50 (nM) ± SD
BOR 84.5 ± 12 (p <0.05)
NER 311 ± 240 (p <0.05)
AFA 395 ± 80 (p <0.05)
ERL 3,330 ± 910
GEF 6,120 ± 390
TAK 5,760 ± 1,300

Figure 5